Urban Heat Under Mediterranean Skies: Comparing Surface Heat Island Patterns in Malta and Zaragoza

Felikss Urga

2026
Department of
Earth and Environmental Sciences
Lund University
Sölvegatan 12
S-223 62 Lund
Sweden

Urban Heat Under Mediterranean Skies: Comparing Surface Heat Island Patterns in Malta and Zaragoza

Felikss Urga

Bachelor thesis, 15 credits, in Physical Geography and Ecosystem Analysis

Supervisor 1, Marko Scholze

Exam committee:
Examiner 1, José Beltrán

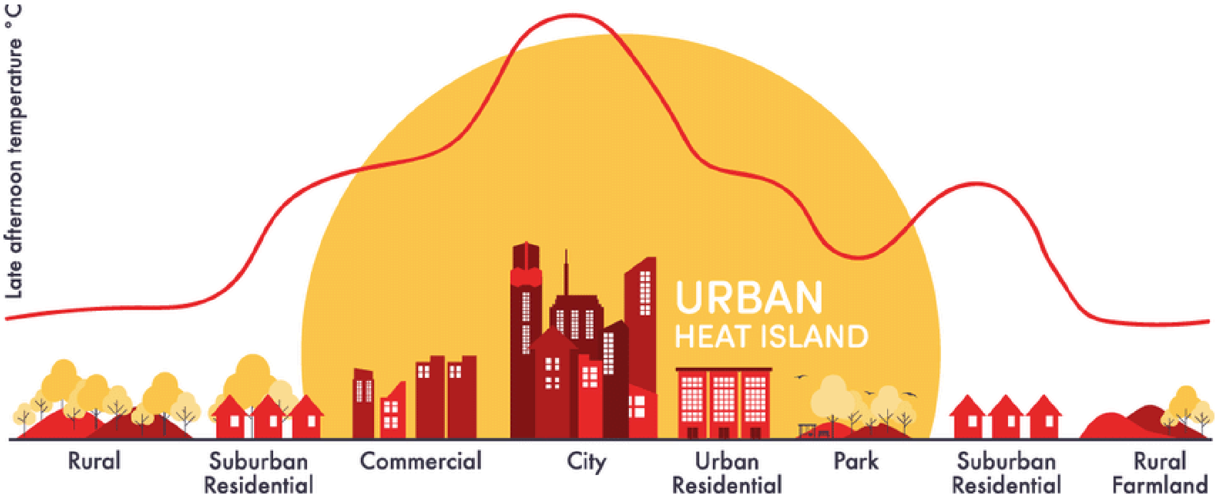

(Image by Kamyar Fuladlu, taken from the World Meteorological Organization, n.d.)

Authors name (2026).
Felikss Urga

Title of thesis (English)
Urban Heat Under Mediterranean Skies: Comparing Surface Heat Island Patterns in Malta and Zaragoza

Title of thesis in Swedish
Stadsvärme under Medelhavets himmel: Jämförelse av ytvärmeömönster på Malta och Zaragoza

Bachelor degree thesis, 15 credits in Physical Geography and Ecosystem Analysis
Department of Physical Geography and Ecosystem Science, Lund University

Level: Bachelor of Science (BSc)

Course duration: *January* 2023 until *June* 2026

Disclaimer

Acknowledgements

I would like to give credit to Marko Schölze for taking on the role of my thesis supervisor and successfully guiding me through this thesis.

This thesis would not be possible without the help and support of my parents. It was through their suggestions and counselling that I decided to start this Bachelor's degree at Lund University, and now I am ecstatic that I will graduate with a Bachelor of Science diploma thanks to them. It is crazy to think how unconditionally they support me, ever since I was a toddler, to this moment in life, and will never stop doing so. Words cannot describe how extremely grateful I am for everything they have done for me.

Thank you, Mom & Thank you, Dad.

Abstract

This study investigates the spatiotemporal development of the Surface Urban Heat Island (SUHI) in Malta, and compares it with Zaragoza, Spain, as an inland reference site of the same Köppen climate classification. High-resolution summer Land Surface Temperature (LST) data from 2013 to 2025, along with Impervious Surface Area (ISA), Land Use/Land Cover (LULC), and NDVI data were used to analyse the SUHI development in the study area. In addition, MODIS day and nighttime LST data from 2003 to 2025 were used to examine a longer-term, diurnal SUHI trends. The results obtained, show that Malta does not display a conventional daytime SUHI signal, as areas defined as rural with ISA were generally warmer than the urban ones, with an urban-rural LST difference of -1.33 °C. In contrast, Zaragoza showed consistently positive urban-rural LST differences of +2.11 °C, indicating a clearer inland SUHI pattern. It was found that MODIS nighttime analysis has resulted in a significant UHI increase in both study areas, +0.019 °C/year in Malta and +0.018 °C/year in Zaragoza. This suggests that urban heat retention is more clearly expressed at night than during the day. Overall, the findings show SUHI development cannot be explained by urbanisation alone; research suggests that factors such as local climate, maritime exposure, vegetation conditions, dry rural surfaces & their composition, along with time of observation, strongly influence how urban heat is expressed.

Table of Contents

1. Introduction

Urbanisation is increasing global exposure to urban climate risks. According to the United Nations Department of Economic and Social Affairs (2018), the proportion of people living in cities has increased from 30% in 1950 to 55% in 2018, and is projected to reach 68% by the year 2050. It is documented that cities create microclimates that are generally warmer than the surrounding areas. This phenomenon is known as the Urban Heat Island (UHI) effect. UHIs are created from the city's heat-retaining properties, geometry, and heat from human activities (Intergovernmental Panel on Climate Change [IPCC], 2021). The basic mechanisms of UHIs are linked to the altered energy balance in cities, which comprises impervious surfaces, dense building materials, and reduced vegetation (Oke, 1982).

1.1 Urban heat relevance and satellite-based monitoring

The relevance of UHIs lies in their capacity to exacerbate heat exposure in already densely populated environments, increasing risks to human health, thermal comfort and livability. This is especially important during periods of prolonged heat and heatwaves. Moreover, studies have demonstrated that UHIs alter precipitation patterns (Shepherd, 2005), and higher urban temperatures can increase cooling-related electricity demand. Santamouris et al. (2015) report that each 1 °C increase in ambient temperature may increase peak electricity demand by 0.45-4.6%, and air-conditioning waste heat can contribute to a positive feedback between urban warming and cooling demand (Takane et al., 2019).

Normally, UHI is subdivided into two categories: the Canopy Urban Heat Island (CUHI), based on air temperature, and the Surface Urban Heat Island (SUHI), based on land surface temperature (LST) (Oke, 1982). Meteorological observations from weather stations can be limited by scarce spatial distribution and their heterogeneity; on the other hand, remote sensing comes into play. It facilitates data provision both spatially and temporally, allowing for continuous data such as LST, Normalised Difference Vegetation Index (NDVI), Land Use Land Cover (LULC), and Impervious Surface Area (ISA). These are crucial components to evaluate the SUHI development in Malta and to compare it with Zaragoza as an inland Mediterranean reference site.

Malta-specific UHI research remains very limited, with existing studies focusing on short-term field measurements, satellite in situ LST comparison, and local mitigation measures. Therefore, a long-term satellite-based study, with a comparison to an inland Mediterranean city with the same Köppen Climate classification, adds value by examining whether the Maltese marine setting modifies the SUHI development over time. This study addresses the gap by comparing Malta with Zaragoza by using consistent LST, NDVI, CLC+ Backbone, and ISA-based workflow.

1.2 Research gap and aims

Aim 1

To investigate the spatiotemporal development & long term spatial trends of the Surface Urban Heat Island (SUHI) from 2013 to 2025 in Malta, using high-resolution Land Surface Temperature data, in conjunction with a stable Land Use/Land Cover mask and impervious surface area classification.

Aim 2

To evaluate the role of maritime influence in shaping SUHI intensity by comparing the thermal characteristics of Malta with Zaragoza, Spain, an inland city sharing the same Köppen Csa climate classification, but without the influence of direct sea-breeze exposure.

Hypothesis 1

This study hypothesises that UHI intensity in Malta has increased significantly over the 2013–2025 period, with urbanisation as the leading cause. As impervious surfaces expand and vegetated land is lost, urban areas are expected to store more heat, release less moisture through evapotranspiration, and reflect less solar radiation — all of which widen the thermal gap between urban and rural areas over time.

Hypothesis 2

This study hypothesises that Malta's island location dampens its UHI intensity compared to a continental city with the same climate type. The sea breeze and higher atmospheric moisture typical of a central Mediterranean island are expected to introduce cooler air into urban areas and reduce heat accumulation, resulting in a measurably lower UHI intensity in Malta than in Zaragoza — even though both cities share the same Köppen Csa classification and similar levels of urban development.

2. Background

2.1 Urban Heat Island Formation

Heat Islands are created due to a combination of several different factors. Reduced natural landscapes in urban areas facilitate the UHI effect. Vegetation and water bodies cool the air by providing shade and by transpiration and evaporation. Artificial surfaces such as roads, roofs and sidewalks, made out of impermeable materials, provide less shade and moisture when compared to their natural counterparts, and therefore lead to higher temperatures (United States Environmental Protection Agency, 2025).

Conventional artificial materials tend to have a higher albedo, therefore absorbing more of the sun's insolation when compared to trees and other natural surfaces. It is documented that heat islands gather up shortwave solar radiation during the day, and later emit this as longwave (thermal) energy during nights and evenings. Hence, creating an even greater UHI when the sun sets (United States Environmental Protection Agency, 2025).

Another cause of UHIs is the anthropogenic heat. Air conditioning units, vehicles, and manufacturing all release heat into the urban environment. These all add up and positively contribute to urban warming (United States Environmental Protection Agency, 2025).

2.2 Urban Geometry and Surface Heat Storage

The way a city is designed plays a major role in how resilient it is to urban heat island (UHI) formation. Spacing between buildings, water bodies, and topography all influence UHI development. Narrow building spacing and street width create a high height-to-width ratio and reduce the sky view factor, thereby limiting the ability of urban surfaces to release longwave radiation at night. Oke (1981, 1982) showed that this can increase nighttime heat retention and contribute to nocturnal UHI development. In contrast, narrow streets can provide more shade during the day and reduce direct solar radiation on pavements and building façades. Therefore, the effect of street width on UHI is time-dependent: wider streets may improve ventilation, but their larger sky view factor can also allow more solar radiation to reach the ground during the day.

UHI can be visualised by drawing a curve from one side of the city to another, therefore mapping geographically the temperature change from rural environment to urban environment and back to rural. The so-called “island” would be the spike in the middle of the graph representing the warmest point, and generally mimics the outline of the urbanised structures (Oke, 1982). Initial studies have revealed that UHI effects can increase urban temperatures between 2 and 8 °C (Oke, 1982; World Meteorological Organisation 1984). However, more recent studies have shown that the more accurate range would be from 5 to 15 °C increase due to the UHI effect (Santamouris, 2013).

2.3 Local Climate, Wind, and Coastal Influence

Local atmospheric and geographic conditions play a big role in the UHI development in cities. The urban atmosphere is divided into two layers. The urban canopy layer, which extends from the ground to roughly the mean roof height; and the urban boundary layer, extending above the roofs upwards to a couple of kilometres, and is influenced by the city below. Each layer directly affects the other; the urban canopy layer contributes heating, cooling, and evapotranspiration to the urban boundary layer, which contributes to the larger mesoscale conditions (Oke, 1982). Oke argues that windspeed is one of the most important meteorological controls of UHI development, followed by cloud cover. Yavuzturk et al. (2005) also show the importance of wind by demonstrating that uninterrupted windflow can increase the heat transfer from asphalt pavements and cool the surface. Zhao et al. (2014) show that the background climate strongly affects UHI intensity. Coastal cities are further complicated by sea land breeze systems, which can cool, shift, or redistribute heat to the atmosphere depending on proximity to shore, shoreline geometry, and the surrounding topography (Hu et al., 2022). In an inland setting, the topography can interact with heat circulation, for example, by bringing cold air down the valleys, potentially intensifying heat stress or restricting circulation (Li et al., 2017; Zheng et al., 2024). Additionally, highlighting the importance of local microclimates, along with usual wind directions, regarding UHI intensity.

2.4 Daytime and Nighttime UHI Behaviour

Daytime and nighttime UHI are controlled by different mechanisms. During the day, LST is strongly influenced by direct solar radiation, surface moisture, vegetation cover, albedo, and the thermal properties of bare soil and artificial materials. Because of this, daytime SUHI does not always produce a simple pattern where urban areas are warmer than rural areas. Extreme summer daytime temperatures may be present in dry arable land, barren land, sparsely vegetated land, and rural land without irrigation. In such instances, the rural comparison area might even experience similar temperatures as the metropolitan area, possibly even higher ones. Such factors affect LST even more than atmospheric temperature, due to the direct dependence of LST upon the surface characteristics observed (Voogt & Oke, 2003; Weng et al., 2004).

At night, the processes controlling UHI are different. After sunset, when direct solar radiation ceases, the contribution of buildings, pavements, and other impervious surfaces to the UHI is linked primarily to the storage and subsequent release of stored heat in the evening. Urban density will reduce the sky view factor in order to minimize the longwave radiation loss, and the material in urban environment usually has high thermal storage capacity. In consequence, the presence of UHI effect at night can occur despite weak, patchy, and possibly masked by rural heat effect during the day (Oke, 1981, 1982). Thus, different components of the same heat system can be described using daytime and nighttime measurements: while daytime LST reflects the quick process of heating, nighttime LST better represents the storage of the heat energy.

This distinction is particularly important for coastal or island environments such as Malta. Coastal urban areas could be moderated by sea-breeze circulation and the surrounding water body, while dry inland rural surfaces may heat rapidly. As a result, daytime urban–rural LST differences can become reduced, or even reversed. In terms of stored heat release from the materials, it is especially noticeable during the night since there is no solar heating during this time. For this reason, analysing both daytime and nighttime SUHI is necessary, as daytime data alone may underestimate or misrepresent the urban heat signal in environments where rural dryness, coastal cooling, and urban heat storage interact.

2.5 Climate Change and the Relevance of Urban Heat Research

Climate change is a long-term shift in Earth’s climate system; it is not just natural variability, but a long-term warming trend strongly linked to mankind's activity (IPCC, 2023). It is caused primarily by anthropogenic greenhouse gas emissions (Forster et al., 2025). The IPCC states that human activities, particularly the emissions of greenhouse gases, have “unequivocally” caused global warming. Such changes in emissions have increased the global surface temperature by approximately 1.1°C above the 1850 - 1900 pre-industrial baseline during 2011-2020 (IPCC, 2023).

Climate change does not stop with just global warming. It strongly affects heatwaves, rainfall patterns, droughts, sea level, ecosystems, and human health (IPCC, 2023; Seneviratne et al., 2021). For that reason, temperature based studies, such as LST and UHI research is becoming increasingly important for understanding how warming interacts with urban land cover and surface conditions (Voogt & Oke, 2003).

It is recorded that the last decade has contained the warmest years in mankind's record (WMO, 2025). The World Meteorological Organisation, among other organisations have confirmed that 2024 was the warmest year on record, averaging out over 1.5°C above the pre-industrial threshold. Additionally, it is reported that 2015 to 2025 were the eleven warmest years in accessible datasets (Copernicus Climate Change Service, 2025; World Meteorological Organization, 2025a).

It is important to note that individual years can be excessively warm, due to natural climate variability such as the El Niño. However, when many record-breaking years occur back-to-back, it is hard to blame the climatic variability. It has become a clear warming trend (IPCC, 2023).

Projections for the future indicate that high temperature records are set to increase over the coming years. According to the IPCC, warming will persist in the absence of significant reductions in greenhouse gas emissions (IPCC, 2023). Global warming between 2081 and 2100 is projected to amount to 1.4°C, 2.7°C, and 4.4°C under scenarios of very low, intermediate, and very high greenhouse gas emissions, respectively (IPCC, 2023). Moreover, the WMO predicts that there is an 80% probability of one year in the range of 2025 to 2029 having a temperature higher than 2024 (World Meteorological Organization, 2025).

3. Data and Methodology

3.1 Study areas

The primary study area is Malta. Malta is a small European island state, located in the Mediterranean Sea at approximately 35.8–36.1°N and 14.2–14.6°E. The archipelago comprises three inhabited islands, Malta, Gozo, and Comino, with a total area of about 316 km^2. Malta is the most densely populated country in Europe, with a population density exceeding 1,500 inhabitants per km^2 (Eurostat, 2022). The country is characterised by a Csa Köppen climate classification, which entails dry summer and mild wet winters (Lionello et al., 2006; Beck et al., 2018). The mean summer temperatures often exceed 25°C, while peak temperatures in urban areas can significantly surpass this value (Climate-Data.org, 2026).

Malta was selected as the primary study site because it provides a spatially compact and clearly bounded case for analysing SUHI development. As an island state, Malta is also geographically separated from neighbouring urban systems, which allows the thermal patterns not to be influenced by surrounding metropolitan areas. In addition to this, Malta’s hot summer Mediterranean climate and high population density make urban heat stress particularly relevant.

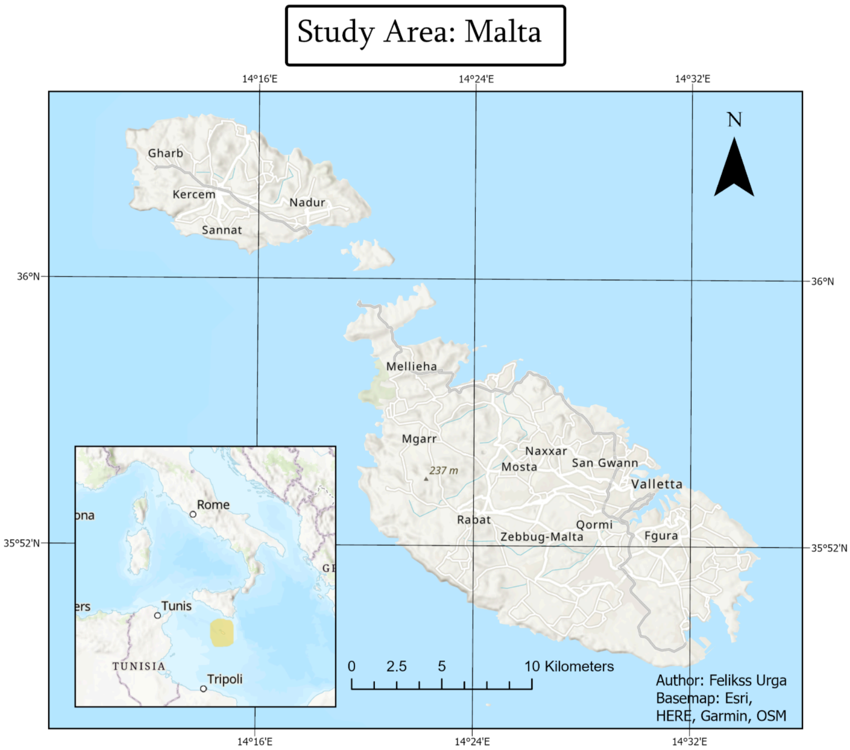

Figure 1. The Maltese study area depicts the whole archipelago with Malta, Gozo, and Comino, along with their location in the Mediterranean Sea.

Malta's rapid urbanisation over the past two decades has resulted in substantial expansion of impervious surfaces, particularly in the populated northern and central regions of the main island, while agriculture, along with natural vegetation, is increasingly fragmented (Planning Authority Malta, 2020). The above-listed information, together with a clearly defined, relatively small spatial extent and intense solar receipt, makes Malta a particularly interesting case for UHI development monitoring.

A Spanish city by the name of Zaragoza, located in the Aragon community, is used as an inland comparison site. The urban satellite site is located 165km from the nearest coastline, therefore it is not exposed to sea breeze the same way Malta is, yet it maintains the same Csa Köppen climate classification. Zaragoza allows for the comparison of the marine and inland climates' effect on UHI development (Beck et al., 2018). For the fairness of this comparison, the same LST, LULC, ISA, and NDVI source and methodology were used on both sites, therefore making the geographical placement the distinguishing factor.

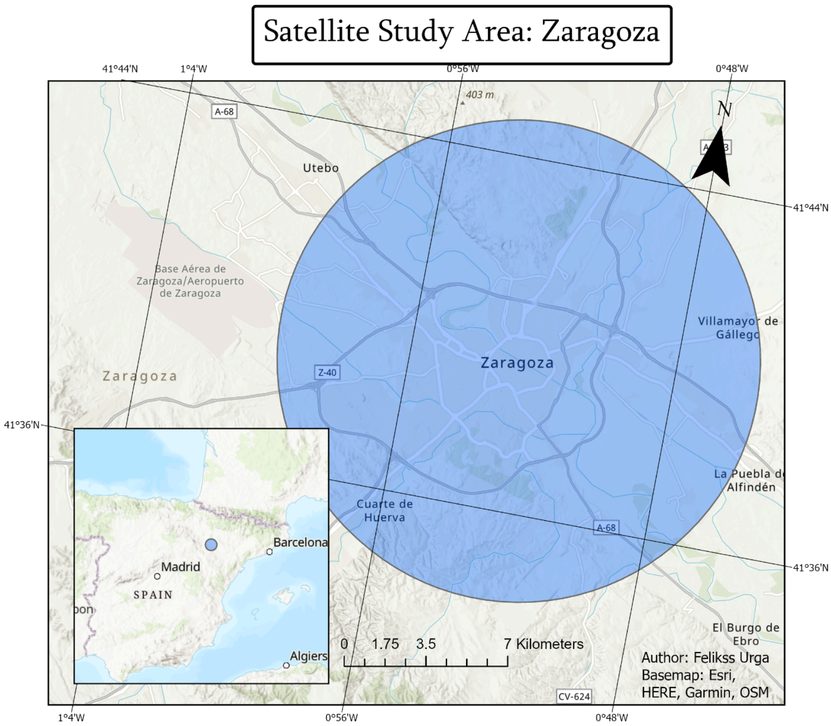

Figure 2. The Zaragoza study area, with its 10km buffer from the Zaragoza city centre. The inserted map shows Zaragoza's inland placement in Northern Spain.

3.2 Data Sources

3.2.1 High-resolution Land Surface Temperature Data

Land Surface Temperature Data at a 30-meter spatial resolution was derived from USGS Landsat 8/9 Collection 2, Level 2 imagery for the period of 2013-2025. To avoid confusion, it is worth mentioning that the LST product is sampled at a 30-meter resolution, however the thermal observations used to retrieve LST are acquired by the Landsat 8/9 TIRS (Thermal Infrared) sensors at 100 meters, and then resampled in the delivered product (U.S. Geological Survey, 2020). Each year, a cloud-free summer scene was selected during the same temporal window (June-August). To ensure spatial compatibility & phenological variation on the LST, same-day data were downloaded from USGS. However, even after filtering for sub 10% cloud cover, some areas were still covered by clouds, which significantly affected LST values, so each image was manually scanned to be cloud-free. If clouds were present, the closest date data was selected, and the process was repeated.

LST was retrieved from TIR bands using the radiative transfer equation approach, which accounts for atmospheric transmittance, upwelling radiance, and land surface emissivity (Jimenez-Munoz et al., 2014). Additionally, surface emissivity was estimated using the NDVI threshold method (Sobrino et al., 2004), whereby emissivity values are assigned based on vegetation fractional cover derived from the Normalised Difference Vegetation Index. The resulting LST rasters were projected to the ETRS89 / UTM Zone 33N coordinate reference system. Additionally, as the initial surface temperatures were shown as integer digital numbers (DN), with pixels ranging from 38209 to 52845, the following equation was used to convert them into degrees Celsius:

$$LST\ (C) = (DN \times 0.00341802 + 149.0) - 273.15 \quad \textbf{\textit{(1):}}\ \textit{Landsat LST conversion}$$

Where DN is the pixel value from the Landsat ST_B10 surface temperature band.

All preprocessing and spatial analysis for high-resolution layers & data were conducted in ArcGIS Pro 3.7 (Esri, 2026).

3.2.2 Normalised Difference Vegetation Index

The Normalised Difference Vegetation Index (NDVI) was computed from the Copernicus browser (European Space Agency, 2026). The Sentinel-2 Level-2A source was used to obtain a 10-meter spatial resolution NDVI output. Unlike the raw, top-of-the-atmosphere reflectance L1C, the L2A is a corrected surface reflectance, and therefore, NDVI was derived from it. The index was calculated using the red band (B04) and the near infrared band (NIR) (B08). NDVI is defined as:

$$NDVI = (NIR - Red) \, / \, (NIR + Red)$$

$$=$$

$$NDVI = (B08 - B04) \, / \, (B08 + B04)$$

***(2):** NDVI formula*

where NIR and Red represent surface reflectance in the near-infrared and red spectral bands, respectively (Tucker, 1979). NDVI values range from −1 to +1, with higher values indicating denser and healthier vegetation cover. NDVI was used both as an input for estimating land surface emissivity and as a vegetation density variable for analysing the spatial relationship between vegetation cover and LST. Such a relationship is a well-established inverse relationship numerously documented in urban remote sensing literature (Yuan & Bauer, 2007; Weng et al., 2004).

3.2.3 Land Use / Land Cover

The LULC data was obtained from the Copernicus Land Monitoring Service Data Viewer (2026) for two different years: 2018 and 2023. The following data was provided at a 10-meter resolution. Only the classes that were present in the official CLC+ Backbone raster were kept, i.e., snow and ice & mosses and lichens were removed.

3.2.4 Impervious Surface Area

Impervious Surface Area (ISA) was used to distinguish between the urban and rural surfaces in both Malta and Zaragoza. The data was obtained from the Copernicus Land Monitoring Service, under the name “Impervious Density 2018 & 2021”. The product is given as a raster file, and provides estimates of artificial surface sealing at 10 spatial resolution, with values ranging from 0% to 100%.

The ISA layers were clipped to the boundary of Malta and Zaragoza. Alike LULC, in order to reduce the influence of land cover change during the study period, a stable mask was created by only including the unchanged areas between 2018 and 2021.

A threshold of 10% imperviousness and above was used to classify the pixels as urban; on the other hand, everything below 10% imperviousness was classified as rural. This threshold was chosen, as even a seemingly low level of impervious surface can indicate built development, such as roads and low-density residual areas. Xian and Crane (2006) used the same threshold, stating that this threshold not only captured the high-density residential areas, but also the low and medium-density ones.

A major benefit of using ISA as a classifier of urban and rural areas is that ISA provides a continuous, quantitative measure of built-up surface intensity, while LULC classes are categorical. The European Union's Earth observation programme, Copernicus Land Monitoring Service (2026) identifies sealed surfaces and built-up construction as important for understanding urbanisation and UHI development.

The use of ISA is also supported by urban heat island literature. For example, Xian and Crane (2006) describe ISA as an anthropogenic parameter representing urban spatial extent and development intensity, and Yuan and Bauer (2007) found a strong linear relationship between LST and percent ISA across seasons. Yuan and Bauer (2007) also found that the LST–ISA relationship was stronger and more consistent than the relationship between LST and NDVI, making ISA particularly suitable for quantitative SUHI analysis, and was therefore used in this study.

3.2.5 MODIS Land Surface Temperature Data

To extend the temporal coverage of the analysis and to examine diurnal UHI dynamics, daily LST data were obtained from the MODIS Terra MOD11A1 product (Collection 6.1) for the period 2003–2025. The MOD11A1 product provides LST at approximately 1-kilometre spatial resolution with separate daytime and nighttime temperature estimates derived from thermal infrared radiance measurements, along wth quality control information, view time, view angle, emissivity and clear sky coverage (Wan et al., 2015; Gorelick et al., 2017). This product has been extensively validated and is widely used in long-term UHI studies (Imhoff et al., 2010; Peng et al., 2012; Clinton & Gong, 2013). The extended temporal record of MODIS data (23 years) provides a long-term context that complements the higher spatial resolution but shorter temporal coverage of the primary Sentinel/Landsat dataset.
Due to the sheer amount of data, that being one nighttime and one daytime measurement for every appropriate summer day from 2003 to 2025, Google Earth Engine (GEE) was used as the data processing software (Google, n.d.). GEE is a cloud-based geospatial analysis platform, in which analysis for Malta and Zaragoza was carried out separately. For the GEE analysis, Artificial Intelligence such as Chat GPT and Claude were used to generate Python scripts to run the necessary SUHI analysis. The code is available in the appendix.

Table 1. Overview of datasets used in the analysis.

Dataset	Source	Spatial resolution	Period/reference years	Use in thesis
Landsat 8/9 Collection 2 Level-2 Surface Temperature	USGS / EROS Centre	30 m delivered grid; thermal retrieval based on TIRS	2013-2025 summer scenes	High-resolution LST maps, Sen slope, MK trend analysis
Sentinel-2 Level-2A NDVI	Copernicus Browser / ESA	10 m	2015-2025 summer scenes	Vegetation-density analysis and LST-NDVI relationship
CLC+ Backbone raster	Copernicus Land Monitoring Service	10 m	2018 and 2023	Official LULC classes and stable LULC mask
Impervious Density HRL	Copernicus Land Monitoring Service	10 m	2018 and 2021	ISA-based urban-rural classification
MODIS Terra MOD11A1	NASA / Google Earth Engine	~1 km	2003-2025 summer days/nights	Long-term daytime and nighttime SUHI trends

3.3 Data Processing

3.3.1 High-resolution data processing in ArcGIS Pro

All high-resolution raster data were clipped to Malta's and Zaragoza's spatial extent before analysis. Zonal statistics as a table were performed in ArcGIS Pro to extract the mean LST values for urban and rural areas.

3.3.2 MODIS Processing in Google Earth Engine

Due to the large volume of daily observations, MODIS LST processing was carried out in GEE. Both sites were processed separately. For each study area, the spatial boundary was imported as a vector, that being Malta's national boundary, and the Zaragoza buffer, in addition to the urban-rural ISA-based classification. These assets were used to filter, clip, and reduce the MODIS image collection.

The daytime LST_Day_1km and nighttime LST_Night_1km bands were selected from each MODIS image. Because the original MODIS LST values are stored as scaled digital numbers, they were converted to degrees Celsius using the standard MODIS scale factor:

$$LST(^\circ C) = (DN \times 0.02) - 273.15$$

***(3):** MODIS LST conversion*

where DN is the stored pixel value from either the daytime or nighttime LST band.

Prior to statistical analysis, quality-control filtering was applied using the MOD11A1 Quality-Control (QC) bands. For both daytime and nighttime LST, pixels with QC bits 0–1 equal to binary 00 or 01 were retained. This meant that pixels were retained where LST was successfully produced under the MODIS mandatory QA_Day and QA_Night flag, and pixels where retrievals were not produced or were of poor quality were excluded. The same QC rule was applied consistently to Malta and Zaragoza to ensure that the two MODIS time series were directly comparable.

The image collection was filtered to the summer months of June, July, and August to ensure seasonal consistency with the high-resolution analysis and to focus on the period when SUHI intensity is strongest. Annual mean summer daytime and nighttime LST composites were generated and exported as GeoTIFF rasters at 1 km resolution for mapping and visual comparison.

Daily summer LST values were also extracted separately for urban and rural areas using the ISA-based urban–rural classification described earlier. Urban areas were defined as pixels with ISA values of 10% or higher, while rural areas were defined as pixels below 10% ISA. Mean LST values were then calculated separately for the urban and rural masks for each available summer day. These daily values were exported as CSV files and used to calculate SUHI intensity:

$$SUHI = LST\ urban - LST\ rural \qquad \textbf{(4):}\ \textit{SUHI formula}$$

This procedure has produced daily, annual, daytime, and nighttime SUHI statistics for both Malta and Zaragoza, thereby allowing comparison between the maritime and inland study areas.

3.4 Statistical Analysis

3.4.1 Mann-Kendall Trend Test

Temporal trends in LST and UHI intensity were assessed using the Mann-Kendall (MK) non-parametric trend test (Mann, 1945; Kendall, 1975). The Mann-Kendall test assesses whether a time series exhibits significant results, without the assumption of normality. Therefore, making it well-suited for environmental time series, which often violate normality, and may contain outliers and missing values (Yue et al., 2002). The test statistic τ ranges from −1 (consistent decreasing trend) to +1 (consistent increasing trend), with values near zero indicating no monotonic trend.

The MK test was applied on two levels. Firstly, it was applied to the high-resolution annual mean UHI series (2013-2025), to assess if a significant long-term trend existed in the time series. Secondly, a pixel-wise MK test was performed on the 13 annual rasters, whereby the test was applied independently on every pixel location to identify the areas of statistically important change. This approach, sometimes referred to as the pixel-based trend analysis, produces maps of trend direction and significance that reveal the spatial heterogeneity of LST change across the study area (de Jong et al., 2011). Pixel-wise MK analysis was implemented in Python using the additionally installed pymannkendall library (Hussain & Mahmud, 2019) within the ArcGIS Pro Jupyter Notebook environment. Statistical significance was defined at the $\alpha = 0.05$ level throughout the analysis.

3.4.2 Sen's Slope Estimator

The magnitude of detected trends was quantified using Sen's Slope estimator (Sen, 1968), a non-parametric method that calculates the median slope across all pairwise combinations of time series values. Sen's Slope is more robust to outliers than ordinary least-squares regression and is the standard complement to the Mann-Kendall test in environmental trend analysis, and was therefore used (Salmi et al., 2002). The estimator yields a slope value in units of °C per year, providing a direct and interpretable measure of the rate of LST change. Pixel-wise Sen's Slope rasters were produced alongside the Mann-Kendall significance maps, enabling spatial quantification of the rate of LST change across the entire Maltese territory. The significance was determined with this code in the raster calculator in ArcGIS Pro:

```
Con("MK_Pvalue.tif" <= 0.05, "MK_Tau.tif", NoData())
```

***(5):** Mann-Kendall Significance*

3.4.3 LST–NDVI and LULC class relationship Analysis

The relationship between vegetation density and surface temperature was examined by computing Pearson's correlation coefficient between pixel-level LST and NDVI values for each year in the study period. This relationship has been consistently reported as negative in urban remote sensing studies, with higher vegetation cover associated with lower surface temperatures due to evapotranspiration and shading effects (Weng et al., 2004; Li et al., 2011). In this study, NDVI was used to provide additional ecological context for interpreting the LST and UHI patterns. Stable LULC classes were also used to compare how different land-cover types corresponded with surface temperature and vegetation patterns in Malta and Zaragoza.

3.4.4 Kruskal-Wallis Test

To determine whether statistically significant differences in mean LST were present between LULC classes, the Kruskal-Wallis H-test was applied (Kruskal & Wallis, 1952). This non-parametric equivalent of one-way ANOVA tests whether two or more independent groups have the same population distribution and is appropriate when the assumption of normality cannot be confirmed, as is common with spatially distributed LST data (McKight & Najab, 2010). This test was applied separately to the two study sites for each annual LST raster. Statistical significance was assessed at $p \leq 0.05$. The purpose of this test was to determine whether LST differed significantly between stable LULC classes, rather than to identify every individual pairwise class difference.

3.4.5 Linear Regression for UHI Trends

In addition to the Mann-Kendall test and the Sen's Slope Estimator, least-squares linear regression was used to describe the direction and strength of annual LST and UHI trends. This process was performed for both the MODIS daytime and nighttime UHI data series and the annual mean high-resolution LST. The slope of regression was used to give the rate of change per annum and was represented in °C annually. The calculated coefficient of determination (R2) shows how well the linear trend accounts for yearly variability & the p-value represents the statistical significance. While linear regression was used as a secondary test and not as the main one, it must be emphasised that climate datasets are usually short, random, and do not follow a normal distribution; hence the assumptions of linear regression are not fully met. Thus, linear regression was applied in this instance to show the trend direction, magnitude, and fit of the data, while Mann-Kendall and Sen's Slope Estimator were more reliable trend methods (Wilks, 2011).

4. Results

This section presents both the spatial and temporal results of the SUHI analysis. First, the ISA-based urban-rural classifications are presented for both study sites. Then, mean LST patterns and annual LST differences between urban and rural classes are presented from the high-resolution dataset. This is followed by pixel-wise Sen's slope and Mann-Kendall trend results, and then a comparison of the long-term MODIS daytime and nighttime UHI trends is presented. Lastly, the NDVI and LST relationship results are put forward and used to describe the vegetation and surface temperature patterns for the interpretation of the SUHI results.

4.1 Spatial classification of urban and rural surfaces

The ISA classification in Figures 3 & 4 shows different spatial structures in Malta and Zaragoza. In the first one, ISA-defined urban pixels are concentrated around the north-east and central parts of the main island, with smaller clusters on Gozo. On the other hand, in Zaragoza, urban pixels form a more compact and continuous pattern around the city centre and the major transport corridor. In both sites, it is observed that the majority of the land is taken up by rural sites, yet the urban pixel arrangement differs. This can be further cross-referenced with Figures 5 & 6, which show all the stable LULC for both study areas.

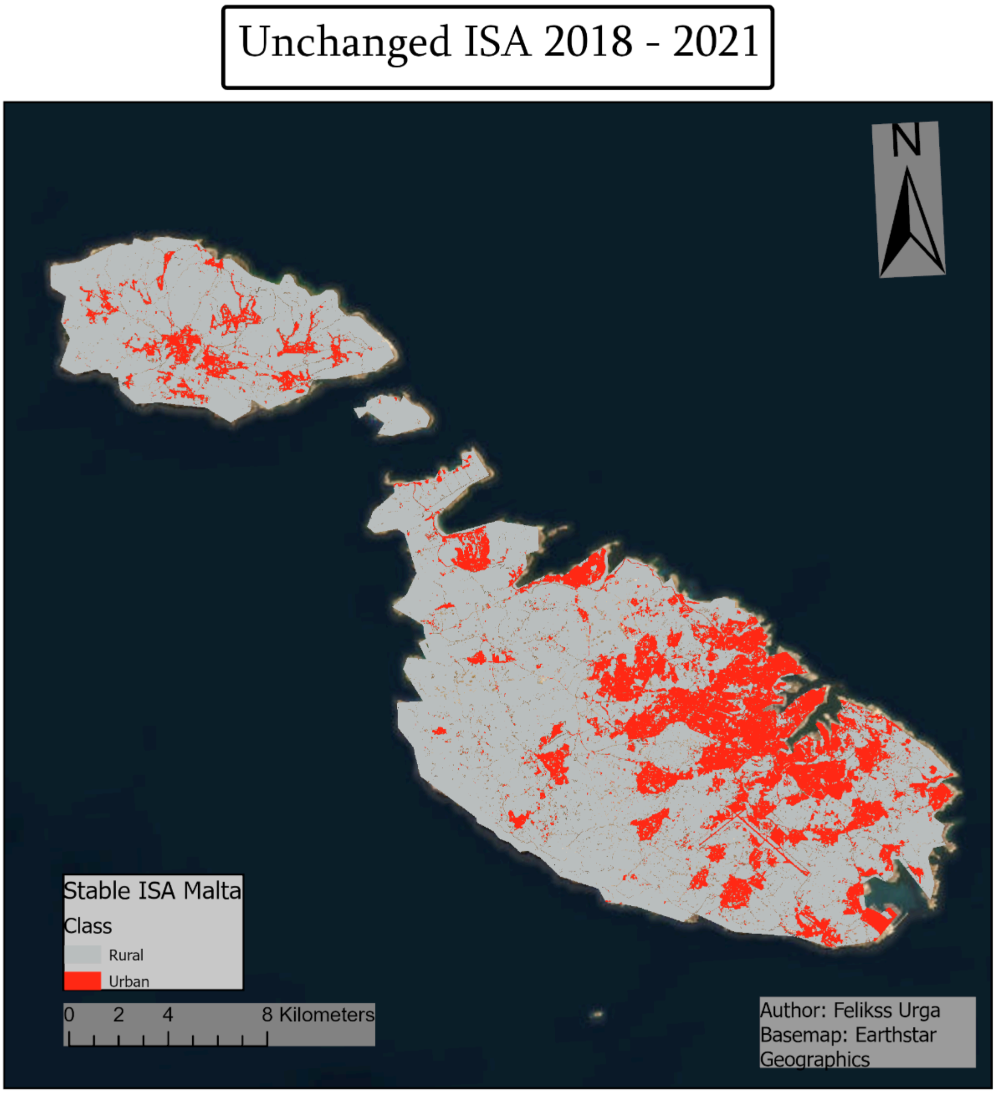

Figure 3. Raster map of the stable ISA in Malta. Only the areas with no ISA percentage change from 2018 to 2021 are shown in the map. The red areas represent the sites classified as urban (ISA above 10%), and are mainly clustered around Valletta in the Northwest of the main island. It is possible to spot the main roads connecting the red areas like a spiderweb. On the other hand, the grey area is classified as urban land with an ISA percentage below 10, and makes up the vast majority of the archipelago's area.

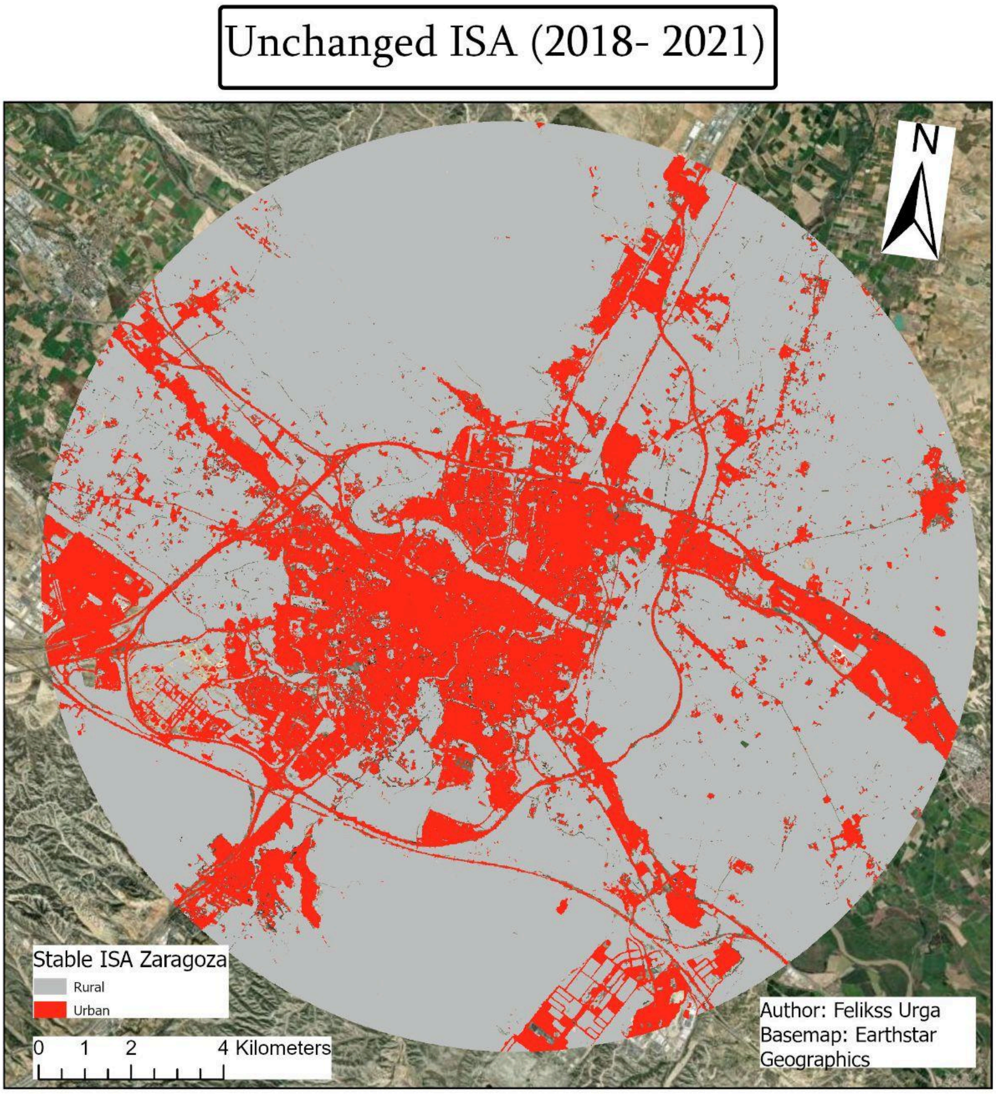

Figure 4. Raster map of the stable ISA in Zaragoza. Only the areas with no ISA percentage change from 2018 to 2021 are shown in the map. The red areas represent the sites classified as urban (ISA above 10%), and are mainly clustered in the middle of the study area, and extend along the major roads. On the other hand, the grey area is classified as urban land with an ISA percentage below 10, which is the majority of the land area.

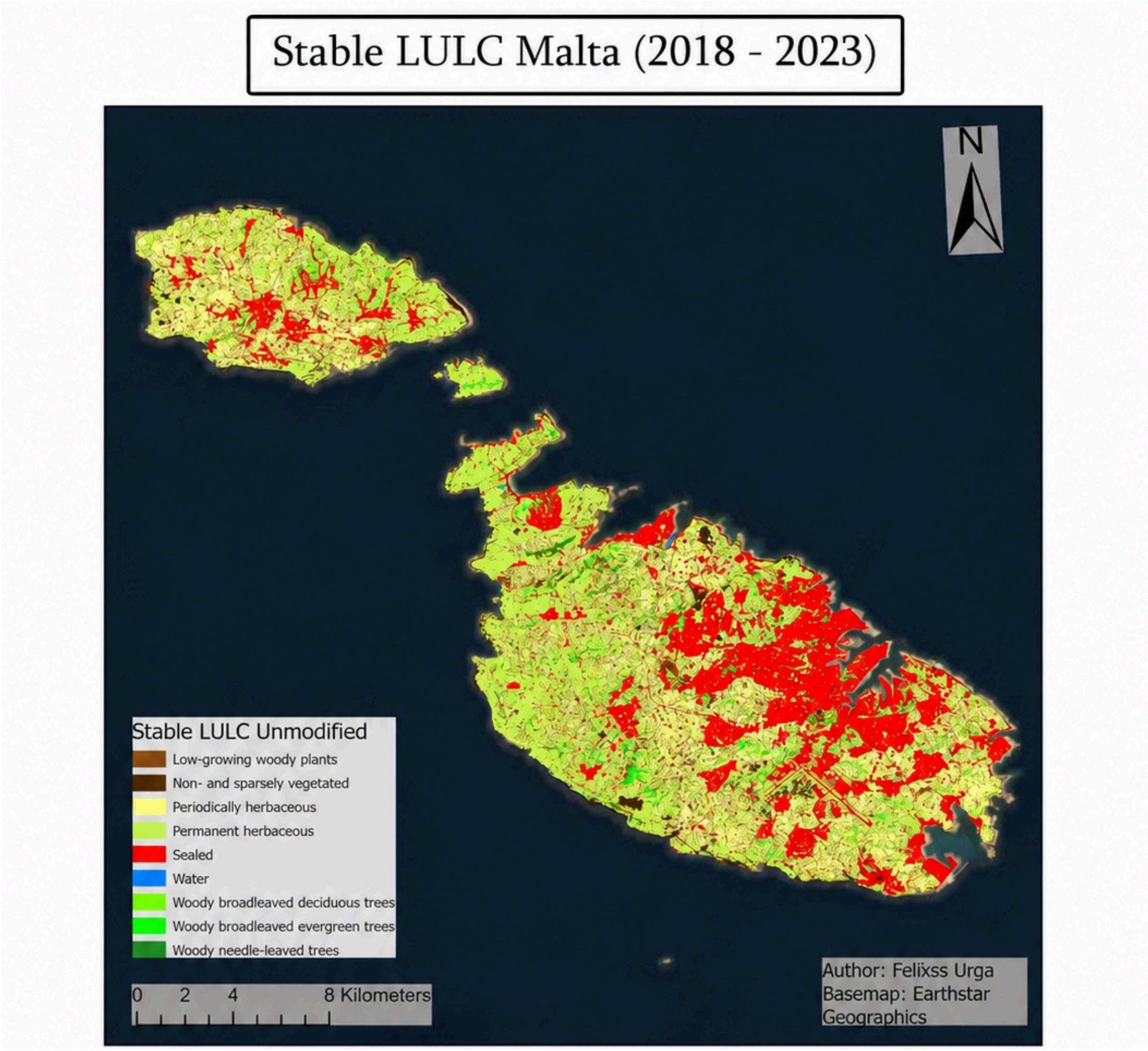

Figure 5. Raster map of the CLC+ Backbone LULC, showing the Land Use / Land Cover for Malta. The stable LULC was created by taking the 2018 and 2023 LULCs and only keeping the areas where no change in LULC was observed. 383,926 pixels changed LULC class out of the 3,091,375 making it 12.42% (10m resolution).

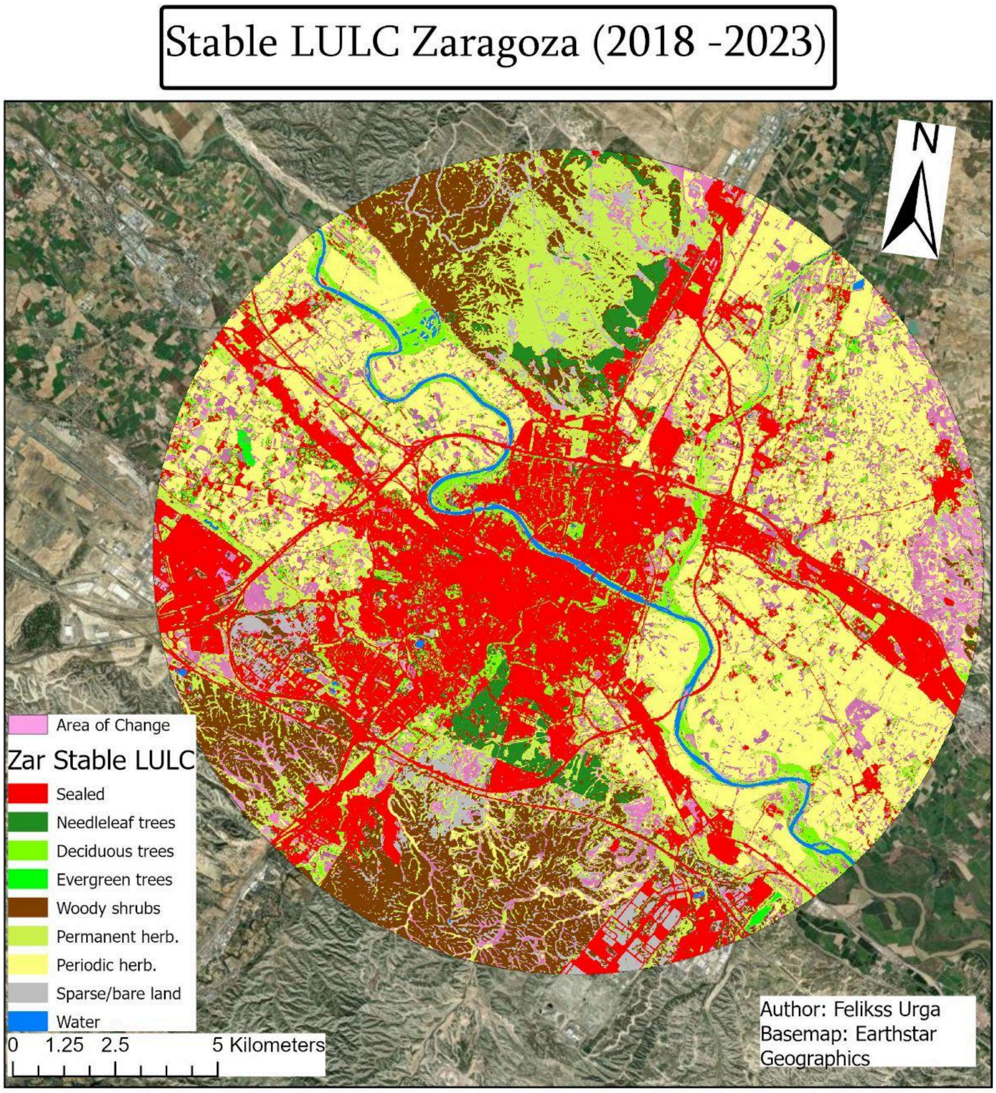

Figure 6. Raster map of the CLC+ Backbone LULC. The map shows the Land Use / Land Cover for the Zaragoza study area. The stable LULC was created by taking the 2018 and 2023 LULCs and only keeping the areas where no change in LULC was observed. 354,074 pixels changed LULC class out of the 3,206,686, making it 11% (10m resolution). To better visualise the areas of change, a bright pink underlayer is present. For a better fit, the LULC names had to be shortened. The full names are: Sealed, Woody needle-leaved trees, Woody broadleaved deciduous trees, Woody broadleaved evergreen trees, Low-growing woody plants, Permanent herbaceous, Periodically herbaceous, Non- and sparsely vegetated, and Water.

4.2 Mean LST patterns and ISA-based urban–rural differences

The mean LST patterns show clearly that thermal variability is present in both areas. In Malta (Figure 7), the highest average LST values occur mainly inland, while lower values are generally located near the coastline. In Zaragoza (Figure 8), high LST values are more widespread into clusters across the area, and cooler zones are agglomerated around the river and vegetated areas. In neither place are the hottest areas located right at the city centres. The island recorded negative urban–rural LST differences in every analysed year, meaning that

ISA-defined rural areas were warmer on average than urban areas. Zaragoza, however, showed the opposite pattern, with consistently positive urban–rural LST differences across all years (Table 2). Lastly, the Kruskal–Wallis test showed significance in LST differences between stable LULC classes in every analysed year for both Malta and Zaragoza ($p < 0.001$). This indicates that land-cover class had a measurable influence on surface temperature patterns in both study areas.

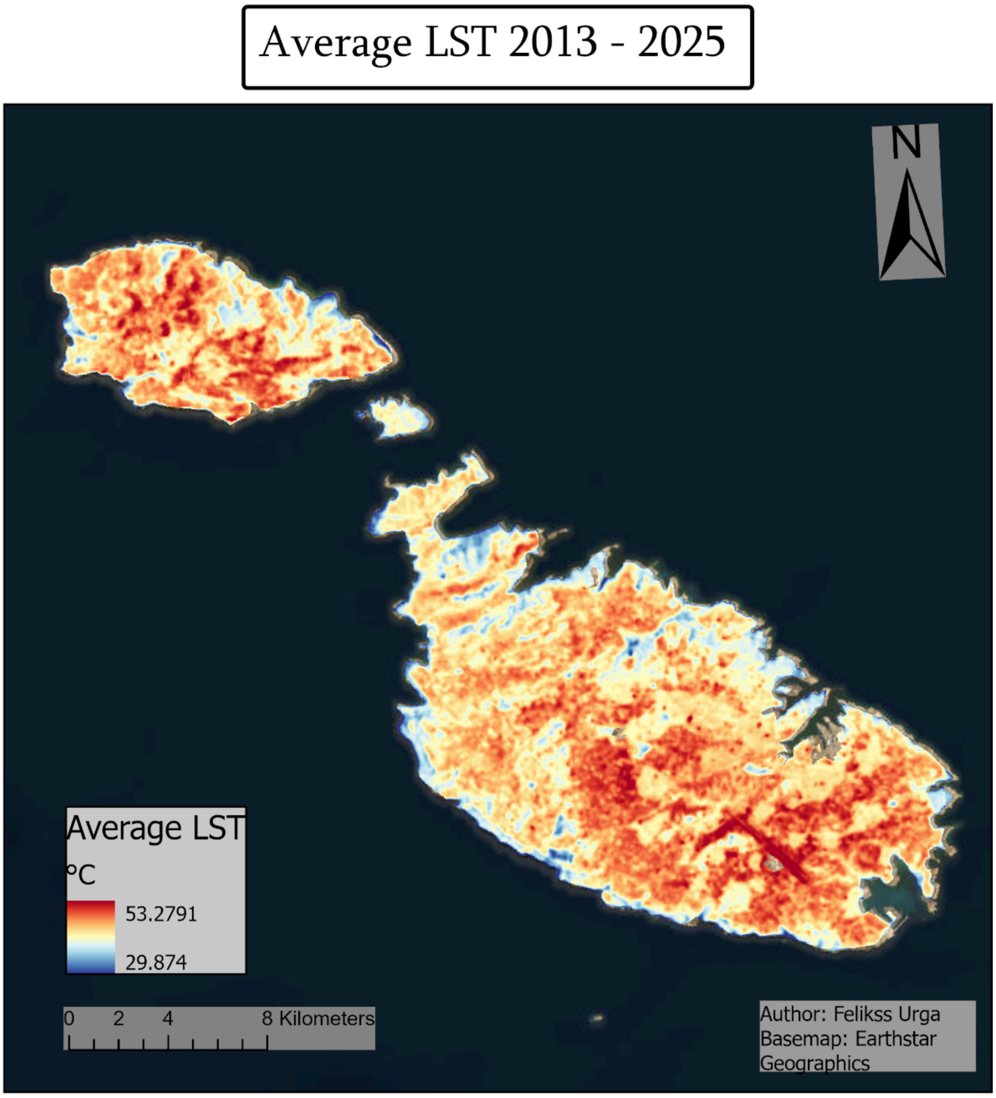

Figure 7. Is a raster map of the averaged LST values in Malta. The yearly summer LST from 2013 up until 2025 was averaged to create an averaged LST map for the Maltese archipelago. The values range from 29.9 to 53.3 degrees Celsius.

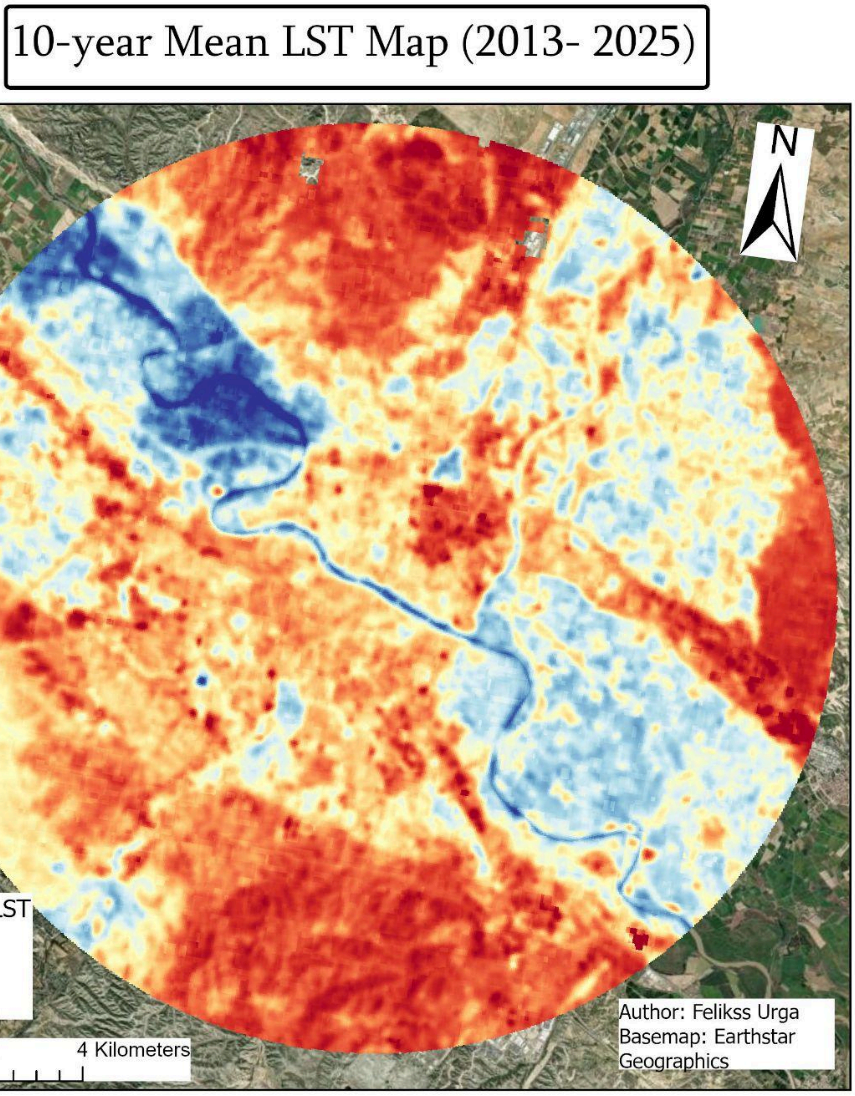

Figure 8. Is a raster map of the averaged LST values in Zaragoza. The yearly summer LST from 2013 up until 2025 was averaged to create a mean LST map for the Zaragoza study area. With values ranging from 25.3 all the way up to 61.1 degrees Celsius.

Table 2. The table shows the ISA-based LST comparison of Malta and Zaragoza, showing that Malta generally had higher rural LST values than urban ones, producing negative urban–rural differences in all analysed years. In contrast, Zaragoza consistently showed higher urban than rural mean LST values, indicating a clearer positive surface urban heat island signal across the full study period. The table with all the yearly values is available in the appendix (Table A1).

Site	**Mean urban–rural difference (°C)**	**Minimum difference (°C)**	**Maximum difference (°C)**	**General pattern**

Malta	-1.33	-2.07 in 2021	-0.27 in 2023	Rural areas are warmer than urban ones
Zaragoza	+2.11	+1.24 in 2015	+4.02 in 2020	Urban areas are warmer than rural ones

Table 3. Showing the Kruskal-Wallis test LST differences between the stable LULC classes for the 2013-2025 time period. Both Malta and Zaragoza sites have shown a p-value < 0.001.

Study area	Years tested	H statistic range	p-value	Significant years
Malta	2013–2025	37,542.50–66,405.43	< 0.001	13/13
Zaragoza	2013–2025	17,758.42–110,076.86	< 0.001	13/13

4.3 High-resolution LST trend analysis

The findings from Pixel-wise Sen's slope show that both study areas have localised warming and cooling tendencies rather than just one uniform trend. In Malta (Figure 9), warming tendencies are mainly visible in parts of the main island, while cooling & weaker trends are visible across large areas of the northern and central part of the archipelago. In Zaragoza (Figure 10), stronger positive results occur mainly in the northern and north-eastern parts of the study area, while negative slopes are present in bunches present in the northwestern and south-eastern parts of the buffer area. The Mann–Kendall significance results (Figures 11 & 12) show that only a small proportion of pixels had statistically significant trends, indicating that many apparent spatial patterns were not monotonic enough across the 13 years to be statistically robust.

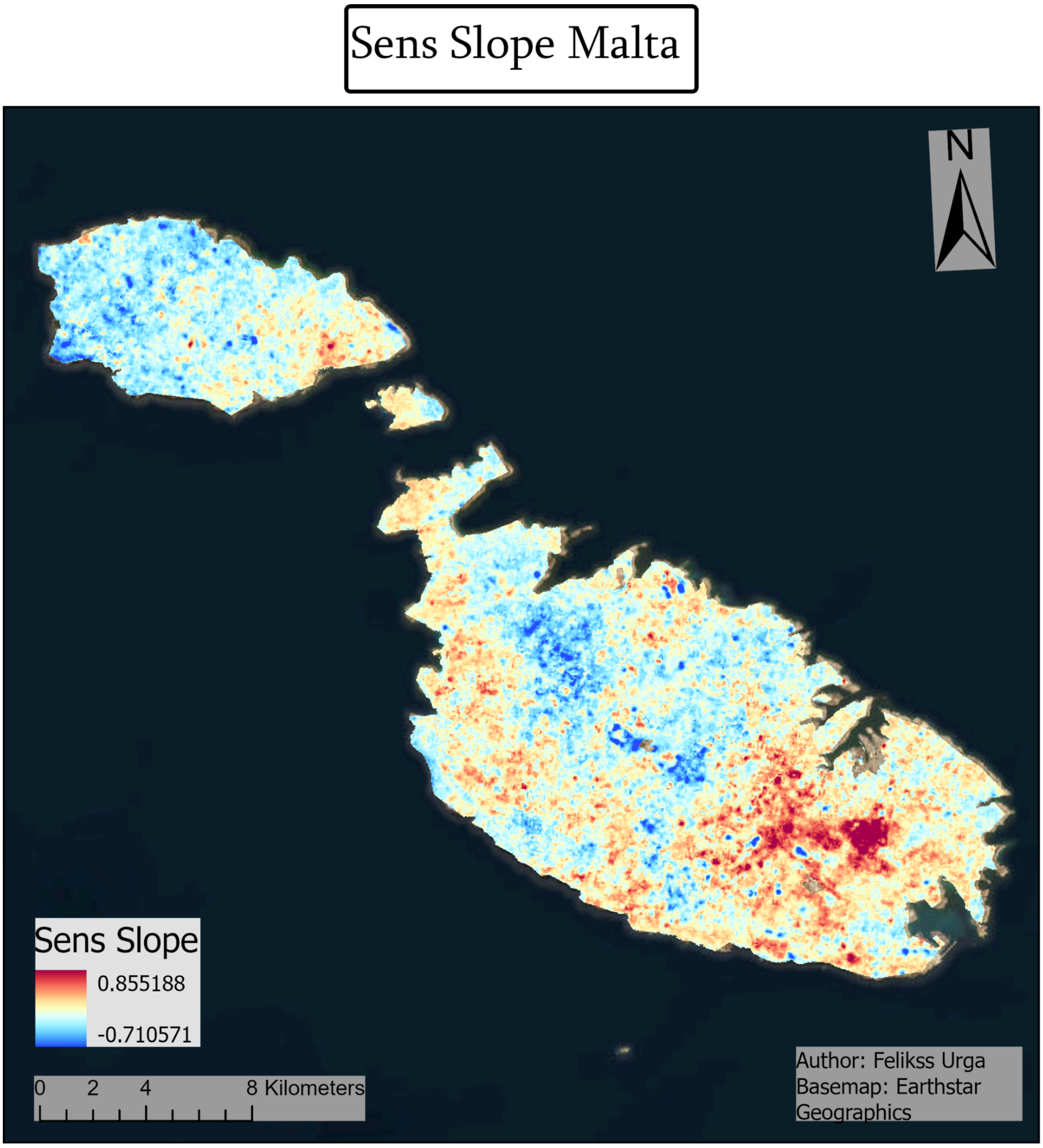

Figure 9. Pixel-wise Sen's Slope of annual land surface temperature in Malta, 2013-2025. The values represent the median annual rate of LST change in °C/year, where positive values indicate warming over the study period, while negative values show cooling.

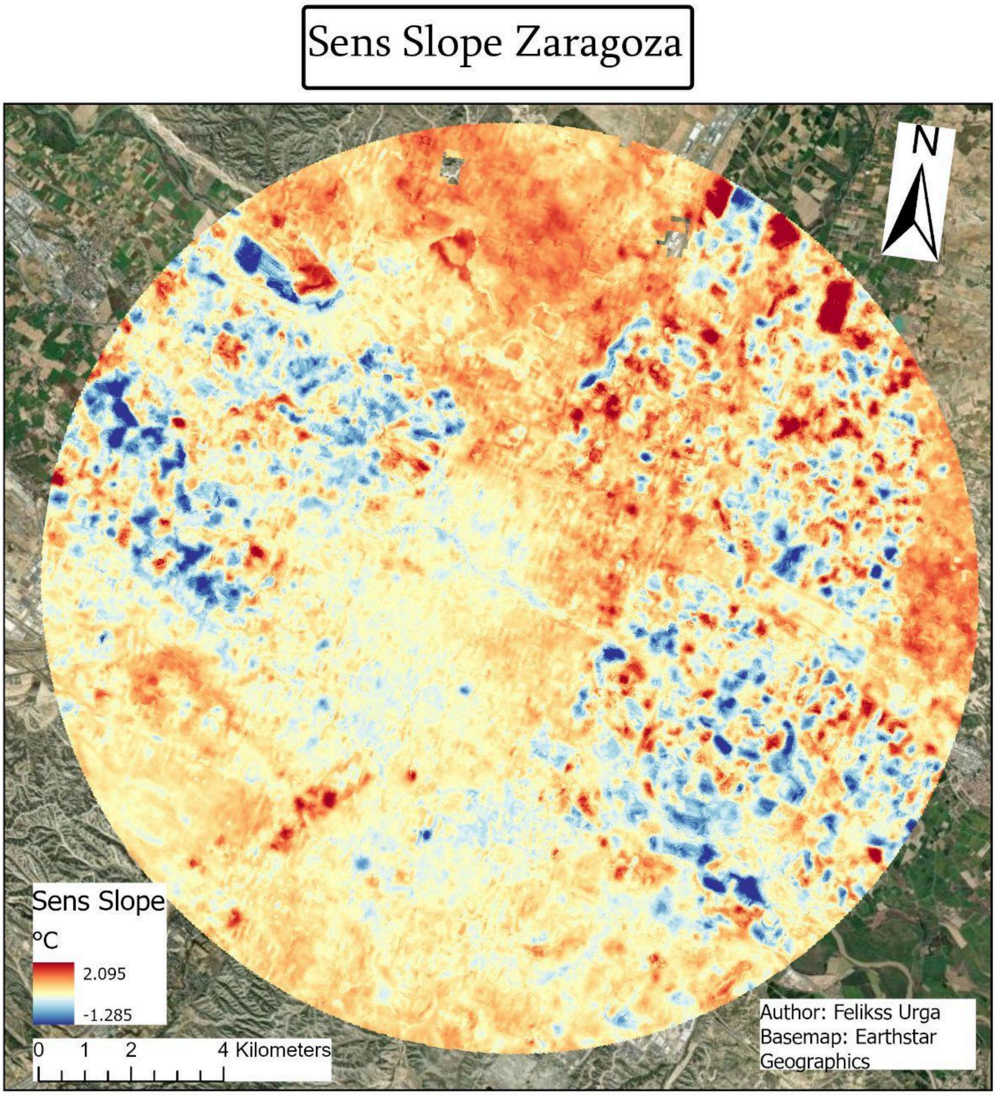

Figure 10. Pixel-wise Sen's Slope of annual land surface temperature in Zaragoza, 2013-2025. The values represent the median annual rate of LST change in °C/year, where positive values indicate warming over the study period, while negative values show cooling.

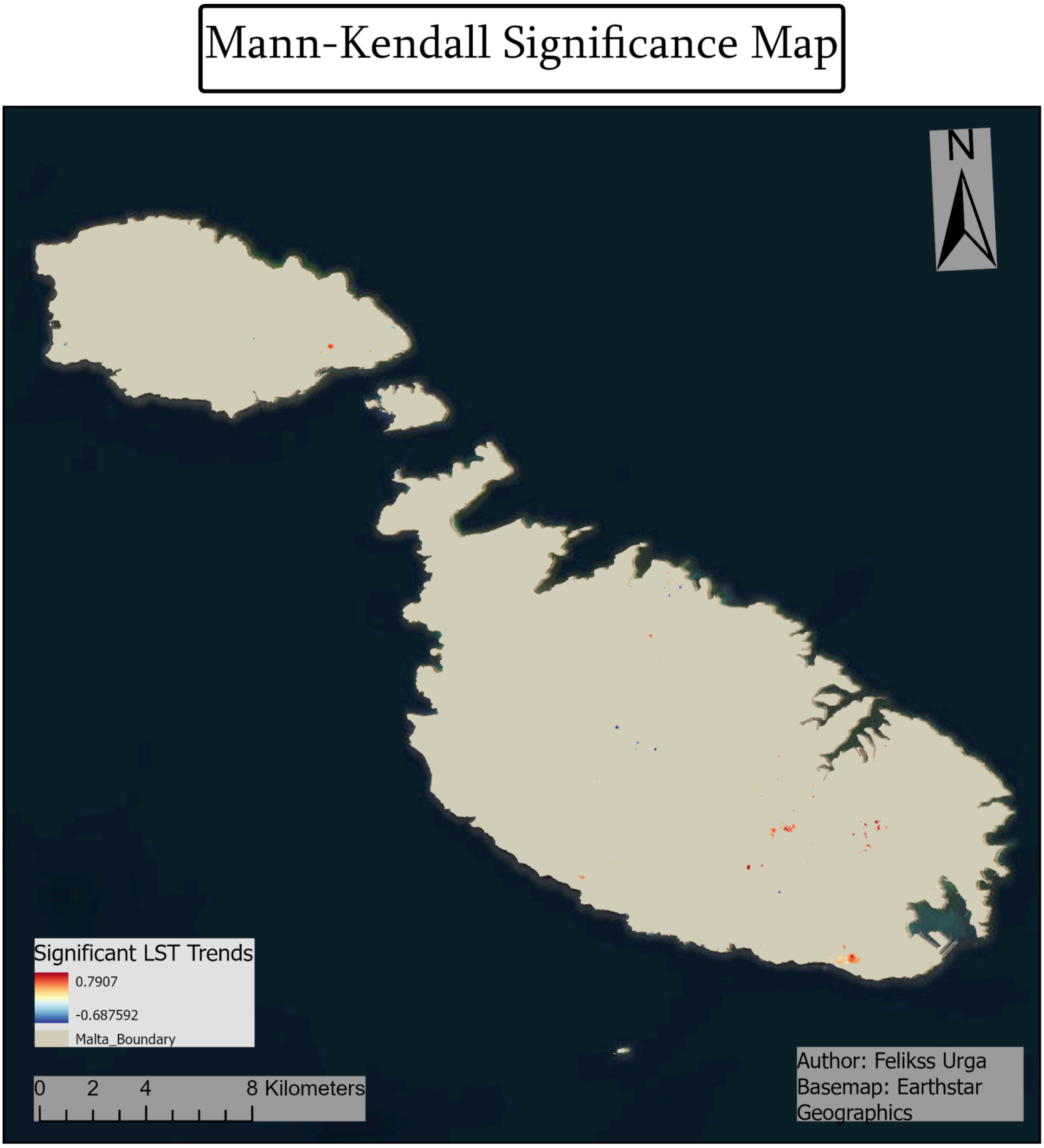

Figure 11. Raster map showing the significant change in LST trends from 2013 up until 2025. A Maltese boundary was placed underneath the Mann-Kendall significance analysis raster to better visualise the few areas of significant change present. The total number of pixels that are considered significant is 756 out of 351,168. If put in percent, this makes it 0.22%. Most of the significant pixels are shown in red, meaning that there has been an increase in temperature. They are primarily located in the lower half of the main island, in industrial-looking areas. Whereas the blue pixels are located in vegetated garden areas inland on the main island.

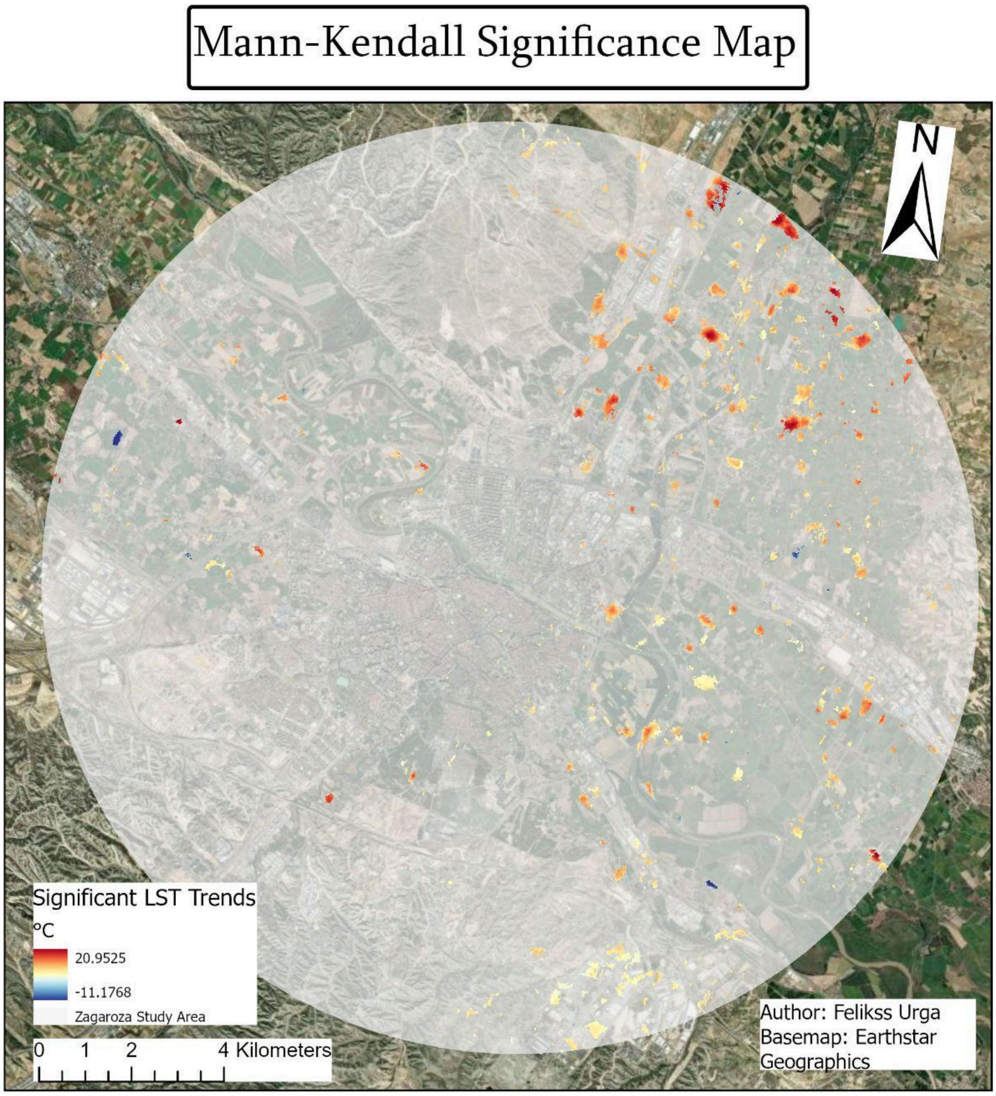

Figure 12. Raster map showing the significant change in LST trends from 2013 up until 2025. A transparent polygon was placed underneath the Mann-Kendall significance analysis raster to better visualise the areas of significant change present. The total number of pixels that are considered significant is 8029 out of 455,621 (30m resolution). If put in percent, this makes it 1.76%. Most of the significant pixels are shown in red, meaning that there has been an increase in temperature. They are primarily located in the eastern half of the study area, with the most prominent ones in the northeast, located in the agricultural fields. Whereas blue pixels are also situated on agricultural fields, however there are less frequent than the red ones, and are scattered around the area.

Table 4. Presents the Mann-Kendall and Sen's slope results for the annual high-resolution urban and rural LSTs classified based on ISA between the years 2013 and 2025. For Malta, none of the tested variables showed significance. While for Zaragoza, the urban mean showed a statistically significant increasing trend, and the rest of the variables did not display significance.

Study area	Variable	Mann–Kendall τ	MK p-value	Sen’s slope (°C/year)	Linear slope (°C/year)	Pearson r	Linear R²	Linear p-value	Significance
Malta	Rural mean LST	-0.0513	0.8577	-0.0130	0.0101	0.023	0.0005	0.9414	Not significant
Malta	Urban mean LST	0.0513	0.8577	0.0308	0.0387	0.093	0.0086	0.7634	Not significant
Malta	Urban − rural LST difference	0.1419	0.5014	0.0387	0.0282	0.174	0.0302	0.5703	Not significant
Zaragoza	Rural mean LST	0.4000	0.0581	0.8376	0.5453	0.508	0.2582	0.0763	Not significant
Zaragoza	Urban mean LST	0.4258	0.0437	0.7242	0.5601	0.543	0.2951	0.0550	Significant increase
Zaragoza	Urban-rural LST difference	0.0513	0.8577	0.0102	0.0140	0.070	0.0049	0.8203	Not significant

4.4 MODIS day & night UHI trends

The MODIS results show a different pattern from the high-resolution daytime analysis. They do so, by separating daytime and nighttime behaviour and looking into how both affect SUHI. In Malta, nighttime UHI increased significantly over the 2003–2025 period, although daytime trend displayed significance, it did so in the negative direction (Figure 13). Zaragoza also showed a significant nighttime UHI increase (Figure 14), however its daytime trend was weaker and not statistically significant in the final trend table, although still negative (Table 5). These results show that the long-term MODIS record captures a clear day–night contrast, with nighttime UHI intensification being the most consistent pattern across both study areas.

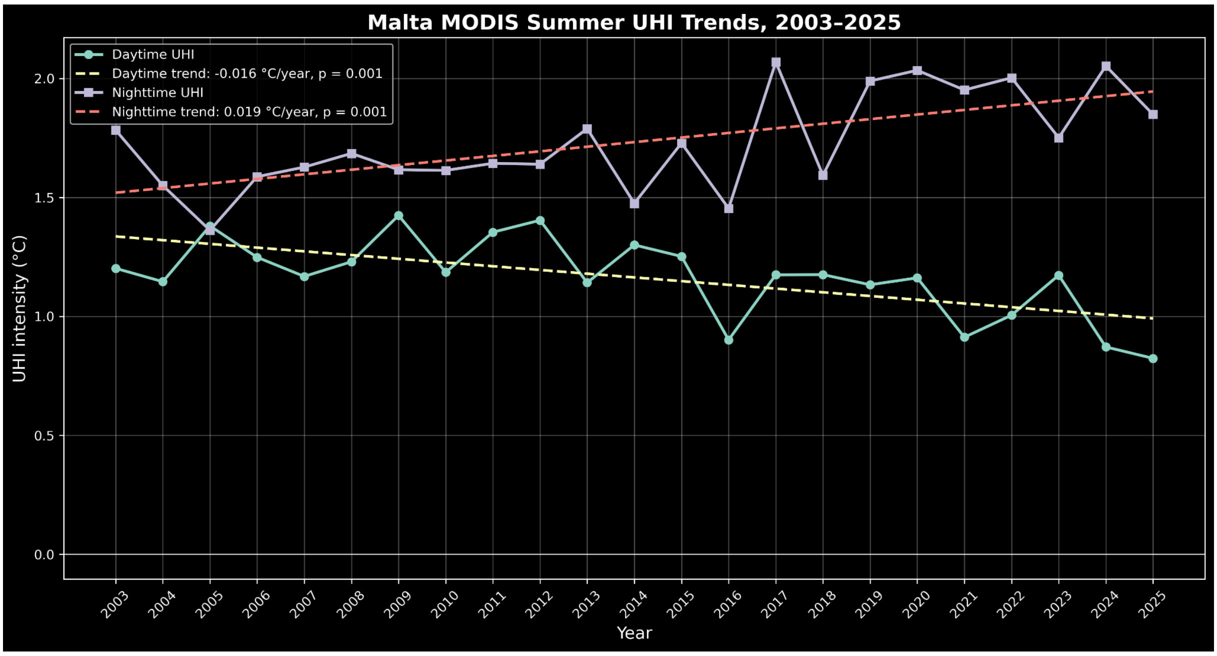

Figure 13. A graph depicting the MODIS UHI trends for the period 2003 to 2025 in Malta. It is visible that the nighttime UHI has a higher intensity (0.019 degrees Celsius per year) than the daytime one, which actually resulted in negative results (-0.016 degrees Celsius per year), both times of the day giving the results with a p-value of 0.001.

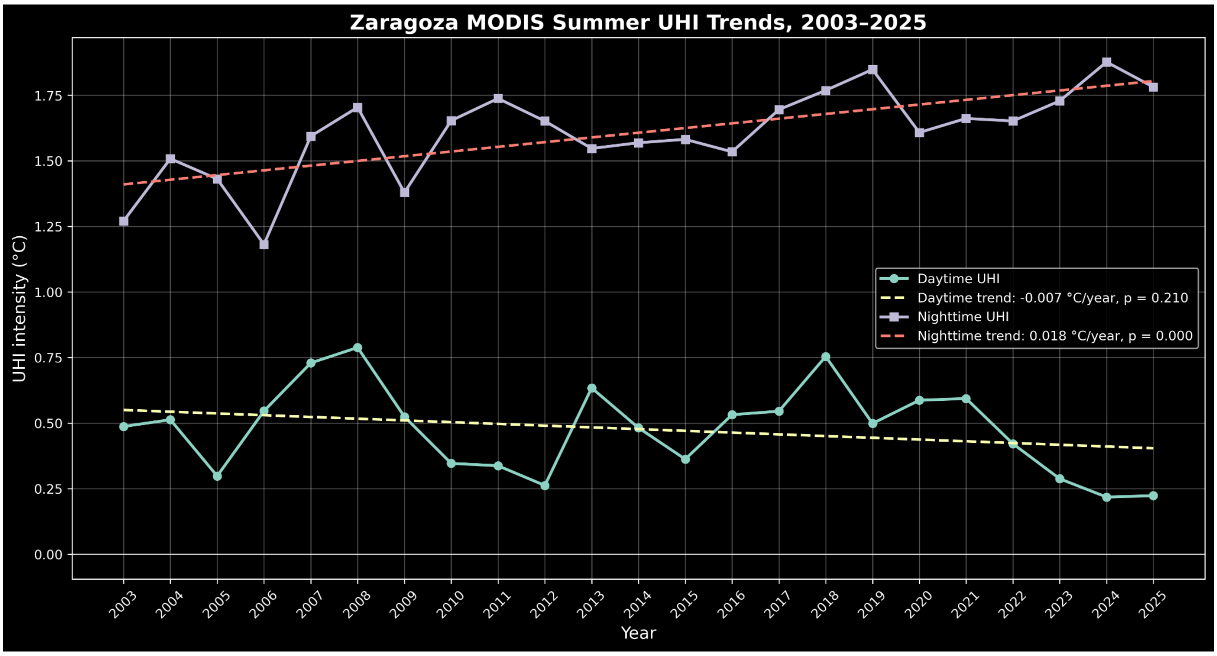

Figure 14. A graph depicting the MODIS UHI trends for the period 2003 to 2025 for Zaragoza. The nighttime UHI is higher intensity (0.018 degrees Celsius per year) than the daytime one, which actually resulted in negative results (-0.007 degrees Celsius per year), and has a p-value of < 0.001 and 0.21, respectively.

Table 5. Trend analysis of MODIS daytime and nighttime UHI in Malta and Zaragoza, 2003-2025. The table summarises the statistical trends, which indicate contrasting daytime and nighttime patterns, with significant nighttime UHI increase in both study areas, a significant daytime decrease in Malta, and no statistically significant daytime trend in Zaragoza.

Study area	UHI period	Linear slope (°C/year)	Pearson r	R^2	p-value	Interpretation
Malta	Daytime UHI	-0.0156	-0.638	0.4071	0.0011	Significant decrease
Malta	Nighttime UHI	+0.0193	+0.639	0.4084	0.0010	Significant increase
Zaragoza	Daytime UHI	-0.0066	-0.2717	0.0738	0.2097	Not significant
Zaragoza	Nighttime UHI	+0.0179	+0.7101	0.5042	0.0001	Significant increase

4.5 NDVI and LST spatial relationships

NDVI patterns provide additional helpful context for the spatial LST differences. In Figure 15, Malta shows lower vegetation values around the main urbanised areas and higher values on Gozo and the western parts of the main island. Zaragoza elucidates the highest NDVI values in riperian and agricultural areas, & lower values in built-up zones (Figure 16). The results show that Zaragoza generally has higher mean NDVI values than Malta across the vast majority of stable land cover classes.

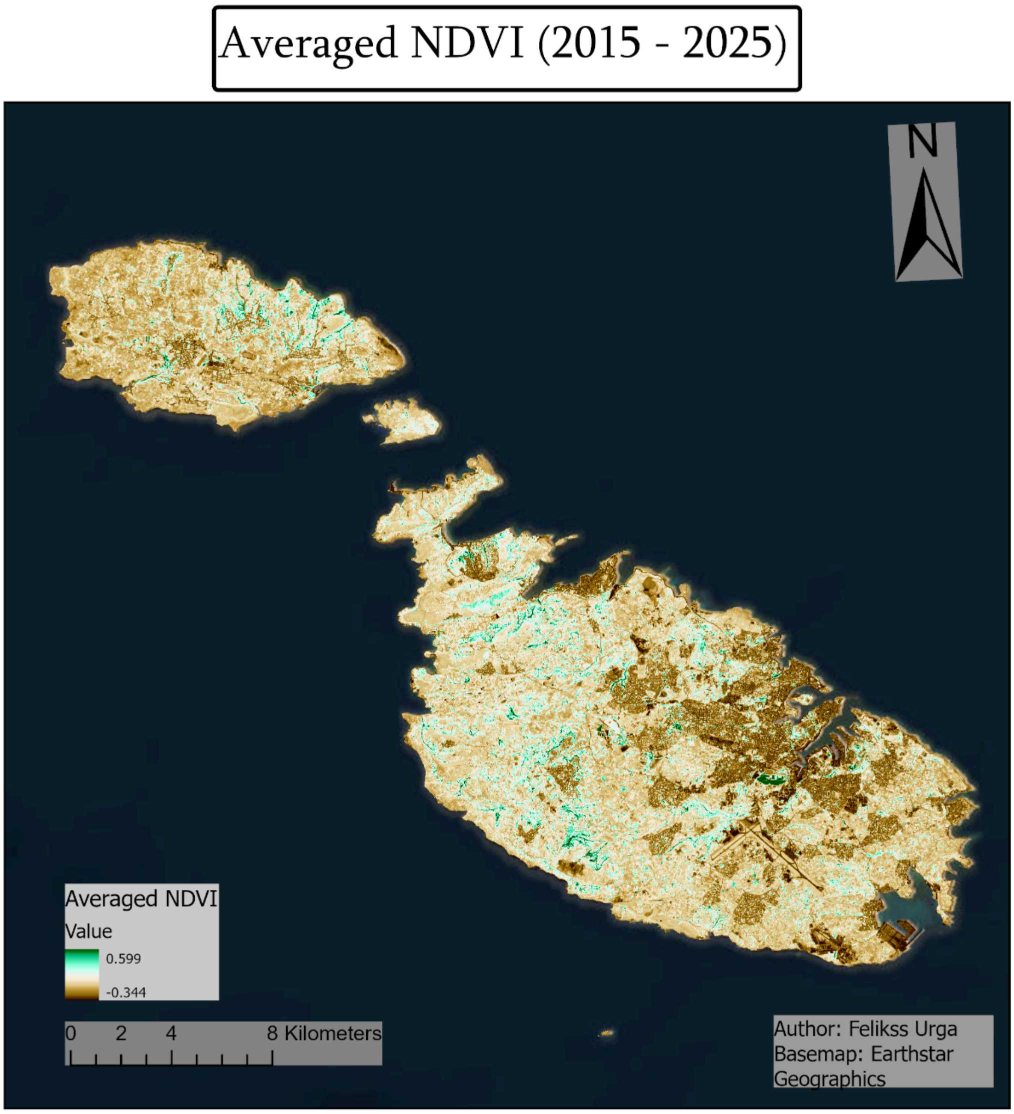

Figure 15. Is a raster map of the averaged NDVI values in Malta. The annual summer NDVI values from 2015 to 2025 were averaged to create a mean NDVI map for the Maltese archipelago. The theoretical range is from -1 to 1. Here we see the values ranging from 0.599 to -0.344. The lowest NDVI values are present around the capital, Valletta, represented by the darker brown colour; on the other hand, the vegetation index is highest in the western part of the biggest island, and the northeast of the northern island.

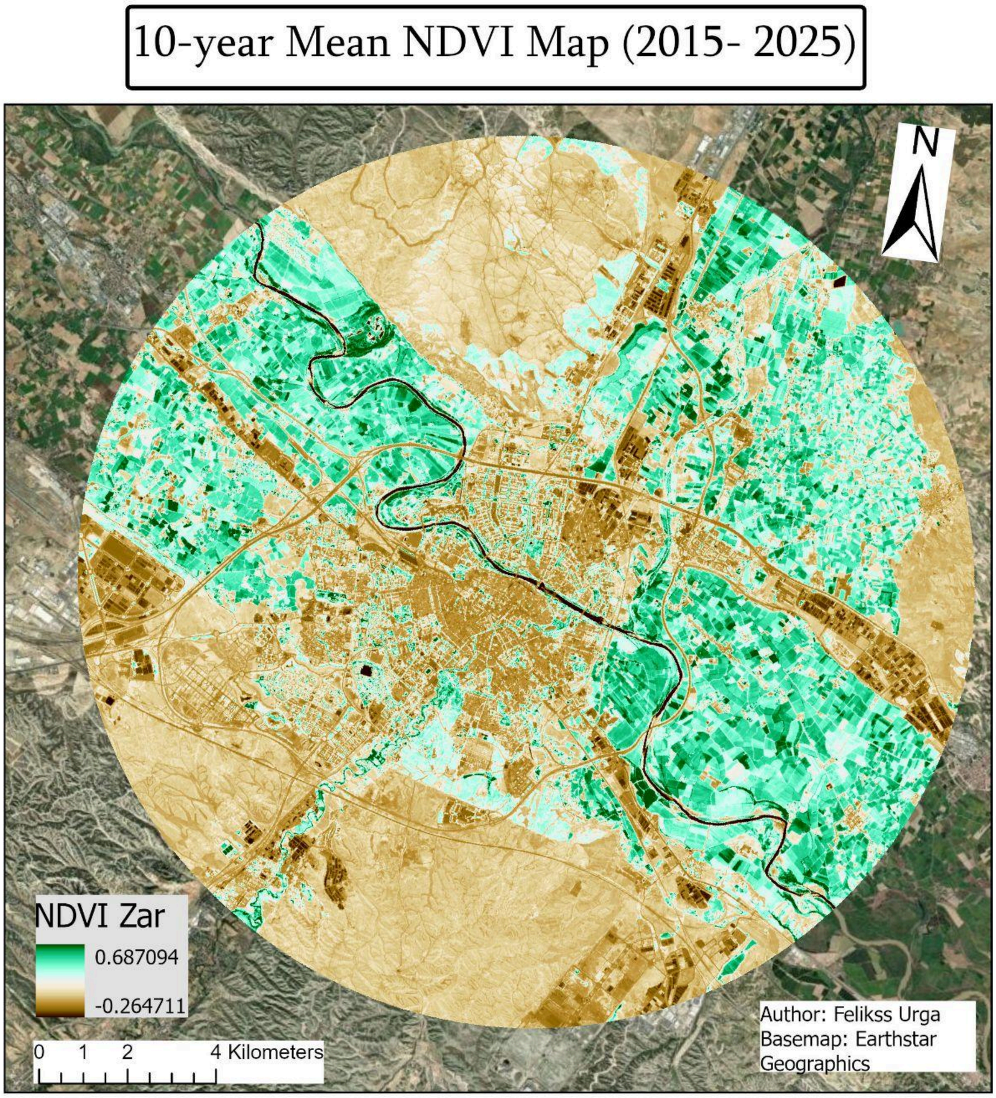

Figure 16. Is a raster map of the averaged NDVI values in Zaragoza. The yearly summer NDVI values from 2015 up until 2025 were averaged to create a mean NDVI map for Zaragoza. The theoretical range is from -1 to 1. Here we see the values ranging from 0.687 to -0.264. The lowest NDVI values are in fact not in the city center, however that is a large area of almost no positive values. They are located in what seems to be industrial buildings close to the edge of the buffer; on the other hand, the vegetation index is highest in the northwestern part, and the southeast of the study area, where lots of agricultural fields are present.

5. Discussion

The results indicate that the development of the surface urban heat island differs substantially between Malta and Zaragoza and cannot be interpreted as a uniform warming pattern. The high-resolution data showed no consistent SUHI when looking at the island site, and only a significant LST increase for the urban sites in Zaragoza. The average LST map shows spatial thermal contrasts; however, the ISA-based urban-rural comparison indicates that Malta has higher rural than urban temperatures, whereas Zaragoza exhibits a contrary, more conventional SUHI signal, indicating a clearer urban surface heat island pattern. However, MODIS data has shown quite different results from the high-resolution data. It adds an important side to the analysis, which shows that nighttime UHI has increased significantly in both study areas, whereas daytime UHI behaved differently.

The Maltese SUHI appears to be weaker and more fragmented than its Zaragoza counterpart, which can be described by the SUHI's sensitivity to marine influence. Such a difference in results supports the claim forwarded by Zhao et al. (2014) that SUHI development is not just controlled by urbanisation, but also by the local climate setting, and climatic parameters such as surface moisture, rural reference conditions, and time of observation.

5.1 Interpretation of Malta's SUHI development

Malta does not show significant daytime SUHI development with the chosen high-resolution ISA method, as visible in Table 5. However, at nighttime, a statistically significant nighttime SUHI development is present.

Additionally, the CLC+ backbone analysis shows that sealed LULC has increased by 5.21% from the time period of 2018 to 2023. Such sealed land is defined by 10m pixels classified as impervious artificial surfaces, including buildings, paved surfaces, asphalt, concrete, tarmacadam, railway tracks, and other open sealed surfaces, with the class assigned through a decision-tree approach where sealed surfaces are evaluated as covering more than 50% of the abiotic component of the pixel (Copernicus Land Monitoring Service, 2024).

Malta's average LST map (Figure 7) shows that the higher LSTs are present inland & far away from the shores, while the coastal areas remain cooler. Build-up areas such as the airport appear to be strong hotspots; however, the ISA-based urban-rural table (Table 2) shows a negative urban- rural difference. Meaning that, contrary to the UHI norms, rural areas in Malta have displayed greater LSTs than the urban ones. Additionally, as seen in Figure 11, the number of significant pixels from the Mann-Kendall analysis is very limited. Statistically significant increase in UHI is observed in the MODIS nighttime UHI in Table 4, with a p-value of 0.001, while the daytime UHI, although displayed significance, was significant in the negative direction, giving a p-value of 0.001.

A likely explanation is that a large portion of rural land in Malta is dry, agricultural land, with exposed soil, and sparse vegetation, as seen in Figure 5. These surfaces are likely to be dry and bare soil, which could have a smaller albedo than the characteristically golden coloured Globigerina limestone, which is a native and primary building material for buildings & structures on the island (Bishop, 2026.). Moreover, the greatest urban area on the archipelago is a harbour city by the name of Valletta. Its proximity to the coast means that Malta's UHI is likely influenced by sea-breeze circulation and the thermal moderation of surrounding water bodies, which can cool coastal urban areas and modify the spatial structure of urban heat islands (Crosman & Horel, 2010; Hu et al., 2022; Zhou et al., 2019). Lastly, the spatial accuracy of the coastal pixels is unknown, so coastal mixed pixels and maritime ventilation lead to a reduction of the urban-rural contrast.

5.2 Maritime influence and comparison with Zaragoza

Table 2, in which the high-resolution ISA-based UHI analysis for Malta has shown negative differences between urban and rural LTSs, meaning that rural areas, on average, had greater temperatures. Whereas the Zaragoza site has shown consistently positive differences in the same parameter and across the same period (Table 2). This comparison indicates that the same ISA-based method produces different thermal results in the two sites, suggesting that geographical placement has a strong influence on how SUHI is developed. Malta's island setting helps explain why its daytime SUHI signal is more complicated than Zaragoza's. Much of Malta's urbanised area is close to the coast, especially around the Valletta harbour region, where sea-breeze circulation and the surrounding water body can moderate daytime surface temperatures and redistribute heat (Crosman & Horel, 2010; Hu et al., 2022; Zhou et al., 2019). At the same time, Malta's rural reference areas often include dry agricultural land, exposed soil, and sparse vegetation, which can become very warm during the daytime conditions in summer. As a result, the urban–rural LST contrast is weakened or even reversed, because urban pixels may be cooled by coastal influence while rural pixels may heat strongly. Zaragoza, in contrast, lacks direct maritime moderation and therefore shows a more conventional inland SUHI pattern.

As mentioned in Section 2.3, sea-breeze circulation is known to affect UHIs by cooling coastal urban areas, shifting heat inland, or redistributing the spatial structure of urban heat rather than producing one fixed hotspot (Hu et al., 2022; Zhou et al., 2019). This is important for Malta, where the main urbanised areas are close to the coast and are therefore more exposed to maritime moderation. Hu et al. (2022) show that UHI and sea-breeze systems can interact dynamically in coastal cities, producing complex spatial heat patterns rather than a simple urban–rural temperature gradient. In contrast, previous studies based on a thermohygrometric sensor network composed of 21 hourly observatories/sensors have shown that Zaragoza has a clear conventional UHI pattern (Barrao et al., 2022). Cuadrat et al. (2022) also found that Zaragoza's UHI is strongest at night and can weaken or nearly disappear under high wind speeds. Therefore, Zaragoza's inland setting produces a more straightforward urban heat pattern, while Malta's coastal exposure makes daytime SUHI more spatially variable and harder to interpret through a simple urban–rural contrast.

5.3 Daytime versus nighttime SUHI behaviour

Daytime LST is strongly affected by parameters like direct solar heating, surface moisture, vegetation condition, bare soil, agriculture, and coastal cooling (Peng et al., 2012; Weng et al., 2004; Yang et al., 2022). This makes daytime SUHI more spatially variable and more sensitive to the local rural reference conditions. In contrast, nighttime UHI is closely built upon the stored heat release of longwave radiation from urban materials and reduced cooling after sunset. Therefore, nighttime MODIS results reveal urban heat retention even when daytime high-resolution results show negative urban-rural differences (Tables 3 & 4). This suggests that daytime LST alone may underestimate the urban heat problem in Malta, and as nighttime heat is affected by the daytime heat accumulation, it is especially relevant as it reduces recovery from daytime heat stress.

5.4 Role of LULC, ISA, and NDVI in explaining spatial patterns

Impermeable Surface Area was used to distinguish and define the urban and rural areas, with a 10% threshold (Figures 3 & 4). Such a method provides better accuracy than traditional LULC classification because ISA is continuous, therefore can be divided into as many subclasses as needed, and represents sealed & artificial surface intensity. ISA has a strong linear relationship with LST as found by Yuan and Bauer (2007), and was more consistent than NDVI for quantitative SUHI analysis. Moreover, there is no human bias on whether to classify some in between LULC as urban or rural, such as parks and similar complicated mixtures of vegetation and built-up areas.

The stable LULC and sealed surface findings are a supportive aid to explain urbanisation, but LULC by itself cannot define the UHI increase. On one hand, the sealed land increases support for physical urban expansion; on the other hand, the thermal results show that expansion is not purely related to daytime SUHI increase in Malta.

The NDVI results show that vegetation patterns differ between the two study areas. In Malta, low vegetation cover in combination with exposed surfaces could explain why rural areas reach high daytime LST values of up to 47 degrees Celsius. In Zaragoza, the much higher NDVI values in the agricultural and riparian zones may explain the presence of cooler areas within the buffer, especially near vegetated and irrigated surfaces. As shown in Figures 15 and 16, NDVI values are lower around the urbanised districts, such as Valletta and the centre of Zaragoza. In addition, when overlayed with Figures 5 & 6, it is visible that NDVI is higher in western/northern vegetated areas on Malta, and in the agricultural zones in Zaragoza; but the agricultural areas can still be thermally complex depending on whether they are naturally or artificially irrigated, and depending on the current season.

5.5 Significance and trend interpretation

The Sen's slope maps, Figures 9 and 10, show the spatiothermal variation in areas that were subjected to warming and cooling, and their respective rates. This confirms the presence of spatial thermal trends despite the few statistical significances of the monotonous trends, which means that the locations experience different interannual temperature regimes. Since statistical significance is more challenging to achieve and due to the fact that the trend analysis at this higher resolution has been conducted using just 13 annual data sets, then such results should not come as a surprise when dealing with short annual time series. While the Sen's slope could determine the warming or cooling tendency, the Mann-Kendall test requires a pattern that is constantly maintained each year. The year-to-year warming or cooling impacts needed to generate more statistical significances of LST trends could be disrupted by the unusually high temperatures seen in recent years alongside their interannual variations.

When comparing the significant pixels of Malta and Zaragoza, the latter has more significant pixels than Malta, although these were still spatially limited relative to the full study area. This indicates that the Sen's slope maps are more useful for visualising the broader spatial pattern and direction of LST change, while the Mann–Kendall significance maps should be interpreted as showing only the areas where those changes were statistically consistent through time. The two outputs should be read together: Sen's slope highlights where warming or cooling tendencies occurred, whereas the Mann–Kendall maps identify where those tendencies were strong enough to be statistically significant. Therefore, areas show apparent warming or cooling in the Sen's slope maps without reaching statistical significance in the Mann–Kendall test.

5.6 Methodological implications and uncertainty

Satellite-derived LST observations should not be interpreted as the same as air temperature. Surface UHI derived from LST represents the thermal behaviour of land surfaces, while canopy UHI is based on near-surface air temperature; these two forms of UHI are related but not identical (Voogt & Oke, 2003). This distinction is important when comparing the results of this study with sensor-based studies of Zaragoza, such as Barrao et al. (2022). Their study used a quality-controlled hourly thermohygrometric sensor network in Zaragoza from March 2015 to February 2021 and identified a clear centre–periphery UHI pattern, with nocturnal intensities exceeding 2 °C. The present study does not contradict those findings. Instead, it supports the existence of a well-developed urban heat signal in Zaragoza, while showing that surface-based SUHI patterns derived from satellite LST can be more spatially heterogeneous and dependent on the time of observation (Barrao et al., 2022; Voogt & Oke, 2003).

The thermal infrared observations used in this study, from Landsat and MODIS, are also limited to clear-sky conditions. This means that the results represent cloud-free summer surface temperature patterns rather than all-weather average conditions. This is important because clear-sky SUHI estimates can differ from all-sky SUHI estimates and may overestimate SUHI intensity, especially during humid summer daytime conditions (Yang et al., 2024).

Another limitation is the spatial resolution of the long-term MODIS LST data. MODIS provided a useful way to analyse daytime and nighttime UHI trends over a 23-year period, but its approximately 1 km pixels contain mixed surface types, including urban land, rural land, vegetation, bare soil, and water. Therefore, the MODIS results should be interpreted as broad long-term thermal patterns rather than detailed local-scale surface temperature conditions (Wan et al., 2021).

Another limitation of this study is that the urban and rural reference areas were classified using a single 10% ISA threshold. This provided a consistent and replicable method for both Malta and Zaragoza, but it also simplified the thermal diversity within each class. In Malta, rural pixels can differ strongly in distance from the sea, elevation, land cover, soil moisture, aspect, and exposure. Some rural areas may therefore consist of dry agricultural land or exposed soil, which can become very warm during summer daytime conditions. Similarly, Zaragoza's rural class includes a mixture of agricultural, vegetated, bare, and possibly irrigated surfaces. As a result, the urban–rural LST difference should be interpreted as a broad ISA-based comparison rather than a complete representation of all local surface conditions. Future research could subdivide urban and rural areas using additional variables, such as distance to coast, elevation, vegetation cover, aspect, soil moisture, or LULC class, to test how different reference definitions affect SUHI intensity.

6. Conclusion

The purpose of this study was to investigate the SUHI development in Malta, at two different spatiotemporal resolutions, and then to compare its thermal behaviour with Zaragoza, an inland site of the same Köppen Climate Classification, which is not so affected by sea air circulation. The results have shown that Malta's SUHI behaviour is not expressed as a simple daytime rural-urban pattern. Malta shows negative high-resolution urban-rural LST differences during the daytime, while long-term MODIS analysis shows a significant nighttime UHI increase. Zaragoza, in contrast, shows a clearer ISA-based SUHI in the high-resolution results.

Hypothesis one is partially supported. Malta has experienced an increase in sealed land, which was attributed to urban; and MODIS analysis showed a significant nighttime UHI increase. Showing that urban heat retention has intensified in Malta across the study period. However, the hypothesis is not fully supported as the high-resolution ISA-based analysis did not show a significant increase in the urban-rural LST difference, and the daytime urban areas on average, were cooler than the rural reference areas. This suggests that urbanisation-related SUHI development in Malta is more clearly expressed through nighttime heat retention than through daytime surface temperature contrasts.

The second hypothesis is broadly supported. The high-resolution ISA-based comparison shows that Zaragoza had positive urban-rural LST differences, indicating a clearer and more conventional SUHI signal than Malta. Supporting the influence of Malta's island setting and exposure to the marine environment on SUHI by dampening its strength. Maritime influence however, does not fully eliminate urban heat accumulation entirely, as both sites displayed significant nighttime SUHIs. It appears to complicate the daytime SUHI while allowing for nighttime heat retention.

Overall, the study demonstrates that the local climate setting and microclimate are crucial for the interpretation of SUHI development. Urbanisation alone cannot be attributed to driving surface temperature patterns, as seen on Malta. UHIs are complex environments, and are affected by a multitude of factors, such as coastal cooling, rural reference conditions, surface dryness, vegetation scarcity, and the difference between daytime heating and nighttime heat release. The comparison with Zaragoza has shown that two cities with the same broad climate classification can show significantly different results in SUHI results, when one is directly influenced by the sea and the other is inland.

7. References

Barrao, S., Serrano-Notivoli, R., Cuadrat, J. M., Tejedor, E., & Saz Sánchez, M. A. (2022). Characterization of the UHI in Zaragoza (Spain) using a quality-controlled hourly sensor-based urban climate network. *Urban Climate, 44*, Article 101207. https://doi.org/10.1016/j.uclim.2022.101207

Beck, H. E., Zimmermann, N. E., McVicar, T. R., Vergopolan, N., Berg, A., & Wood, E. F. (2018). Present and future Köppen-Geiger climate classification maps at 1-km resolution. *Scientific Data, 5*, Article 180214. https://doi.org/10.1038/sdata.2018.214

Bishop, A. (2026). *Limestone country: The story behind Malta's iconic golden hue*. GuideMeMalta.com. https://www.guidememalta.com/en/limestone-country-the-story-behind-malta-s-iconic-golden-hue

Climate-Data.org. (n.d.). *Climate: Malta*. Retrieved May 13, 2026, from https://en.climate-data.org/europe/malta-178/

Clinton, N., & Gong, P. (2013). MODIS detected surface urban heat islands and sinks: Global locations and controls. *Remote Sensing of Environment, 134*, 294–304. https://doi.org/10.1016/j.rse.2013.03.008

Copernicus Climate Change Service. (2025, January 10). *Copernicus: 2024 is the first year to exceed 1.5°C above pre-industrial level*. European Centre for Medium-Range Weather Forecasts. https://climate.copernicus.eu/copernicus-2024-first-year-exceed-15degc-above-pre-industrial-level

Copernicus Data Space Ecosystem. (n.d.). *Copernicus Browser* [Data browser]. Retrieved May 13, 2026, from https://browser.dataspace.copernicus.eu/

Copernicus Land Monitoring Service. (n.d.). *Data viewer* [Web application]. Retrieved May 13, 2026, from https://land.copernicus.eu/en/map-viewer

Copernicus Land Monitoring Service. (2024). *CLC+ Backbone 2023: Product user manual*. European Environment Agency. https://land.copernicus.eu/en/technical-library/product-user-manual-clcplus-backbone-2023-1

Copernicus Land Monitoring Service. (2025). *CLCplus Backbone 2021: Product user manual*. European Environment Agency. https://library.land.copernicus.eu/products/CLCplus_Backbone_2021_PUM_v1.html

Copernicus Land Monitoring Service. (2026). *High Resolution Layer Imperviousness*. Retrieved May 13, 2026, from https://land.copernicus.eu/en/products/high-resolution-layer-imperviousness

Crosman, E. T., & Horel, J. D. (2010). Sea and lake breezes: A review of numerical studies. *Boundary-Layer Meteorology, 137*(1), 1–29. https://doi.org/10.1007/s10546-010-9517-9

Cuadrat, J. M., Serrano-Notivoli, R., Barrao, S., Saz, M. Á., & Tejedor, E. (2022). Variabilidad temporal de la isla de calor urbana de la ciudad de Zaragoza (España). *Cuadernos de Investigación Geográfica, 48*(1), 97–110. https://doi.org/10.18172/cig.5022

de Jong, R., de Bruin, S., de Wit, A. J. W., Schaepman, M. E., & Dent, D. L. (2011). Analysis of monotonic greening and browning trends from global NDVI time-series. *Remote Sensing of Environment, 115*(2), 692–702. https://doi.org/10.1016/j.rse.2010.10.011

Earth Resources Observation and Science Center. (2020). *Landsat 8–9 Operational Land Imager and Thermal Infrared Sensor Collection 2 Level-1 data* [Data set]. U.S. Geological Survey. https://www.usgs.gov/centers/eros/science/usgs-eros-archive-landsat-archives-landsat-8-9-operational-land-imager-and

Esri. (2026). *ArcGIS Pro* (Version 3.7) [Computer software]. https://www.esri.com/en-us/arcgis/products/arcgis-pro/overview

European Union, Copernicus Land Monitoring Service. (n.d.). *Imperviousness Change 2018–2021: Raster 20 m and 100 m, Europe, 3-yearly* [Data set]. Retrieved May 13, 2026, from https://land.copernicus.eu/en/products/high-resolution-layer-imperviousness/imperviousness-density-change-2018-2021

Eurostat. (2024). *Demography of Europe – 2024 edition*. European Commission. https://ec.europa.eu/eurostat/web/interactive-publications/demography-2024

Fensholt, R., & Proud, S. R. (2012). Evaluation of Earth observation based global long-term vegetation trends: Comparing GIMMS and MODIS global NDVI time series. *Remote Sensing of Environment, 119*, 131–147. https://doi.org/10.1016/j.rse.2011.12.015

Forster, P. M., Smith, C., Walsh, T., Lamb, W. F., Lamboll, R., Cassou, C., Hauser, M., Hausfather, Z., Lee, J.-Y., Palmer, M. D., von Schuckmann, K., Slangen, A. B. A., Szopa, S., Trewin, B., Yun, J., Gillett, N. P., Jenkins, S., Matthews, H. D., Raghavan, K., ... Zhai, P. (2025). Indicators of global climate change 2024: Annual update of key indicators of the state of the climate system and human influence. *Earth System Science Data, 17*, 2641–2686. https://doi.org/10.5194/essd-17-2641-2025

Fuladlu, K. (n.d.). *Urban heat island* [Image]. In World Meteorological Organization, *Urban heat island*. https://public.wmo.int/urban-heat-island

Google. (n.d.). *Earth Engine Code Editor*. Google for Developers. Retrieved May 27, 2026, from https://developers.google.com/earth-engine/guides/playground

Gorelick, N., Hancher, M., Dixon, M., Ilyushchenko, S., Thau, D., & Moore, R. (2017). Google Earth Engine: Planetary-scale geospatial analysis for everyone. *Remote Sensing of Environment, 202*, 18–27. https://doi.org/10.1016/j.rse.2017.06.031

Grammarly. (n.d.). Grammarly for Microsoft Word [Writing assistance software]. Retrieved May 27, 2026, from https://www.grammarly.com/microsoft-word

Hu, Y., Tan, J., Grimmond, S., Ao, X., Yan, Y., & Liu, D. (2022). Observed and modeled urban heat island and sea-breeze circulation interactions: A Shanghai case study. *Journal of Applied Meteorology and Climatology, 61*(3), 239–259. https://doi.org/10.1175/JAMC-D-20-0246.1

Hussain, M. M., & Mahmud, I. (2019). pyMannKendall: A Python package for non-parametric Mann Kendall family of trend tests. *Journal of Open Source Software, 4*(39), Article 1556. https://doi.org/10.21105/joss.01556

Imhoff, M. L., Zhang, P., Wolfe, R. E., & Bounoua, L. (2010). Remote sensing of the urban heat island effect across biomes in the continental USA. *Remote Sensing of Environment, 114*(3), 504–513. https://doi.org/10.1016/j.rse.2009.10.008

Intergovernmental Panel on Climate Change. (2021). *Climate change 2021: The physical science basis. Contribution of Working Group I to the Sixth Assessment Report of the Intergovernmental Panel on Climate Change*. Cambridge University Press. https://doi.org/10.1017/9781009157896

Intergovernmental Panel on Climate Change. (2023). Summary for policymakers. In H. Lee & J. Romero (Eds.), *Climate change 2023: Synthesis report. Contribution of Working Groups I, II and III to the Sixth Assessment Report of the Intergovernmental Panel on Climate Change* (pp. 1–34). IPCC. https://doi.org/10.59327/IPCC/AR6-9789291691647.001

Jiménez-Muñoz, J. C., Sobrino, J. A., Skoković, D., Mattar, C., & Cristóbal, J. (2014). Land surface temperature retrieval methods from Landsat-8 thermal infrared sensor data. *IEEE Geoscience and Remote Sensing Letters, 11*(10), 1840–1843. https://doi.org/10.1109/LGRS.2014.2312032

Kendall, M. G. (1975). *Rank correlation methods* (4th ed.). Charles Griffin.

Kruskal, W. H., & Wallis, W. A. (1952). Use of ranks in one-criterion variance analysis. *Journal of the American Statistical Association, 47*(260), 583–621. https://doi.org/10.1080/01621459.1952.10483441

Li, M., Wang, T., Xie, M., Zhuang, B., Li, S., Han, Y., & Cheng, N. (2017). Modeling of urban heat island and its impacts on thermal circulations in the Beijing–Tianjin–Hebei region, China. *Theoretical and Applied Climatology, 128*, 999–1013. https://doi.org/10.1007/s00704-016-1903-x

Li, J., Song, C., Cao, L., Zhu, F., Meng, X., & Wu, J. (2011). Impacts of landscape structure on surface urban heat islands: A case study of Shanghai, China. *Remote Sensing of Environment, 115*(12), 3249–3263. https://doi.org/10.1016/j.rse.2011.07.008

Lionello, P., Malanotte-Rizzoli, P., & Boscolo, R. (Eds.). (2006). *Mediterranean climate variability*. Elsevier. https://doi.org/10.1016/S1571-9197(06)80003-0

Mann, H. B. (1945). Nonparametric tests against trend. *Econometrica, 13*(3), 245–259. https://doi.org/10.2307/1907187

McKight, P. E., & Najab, J. (2010). Kruskal-Wallis test. In I. B. Weiner & W. E. Craighead (Eds.), *The Corsini encyclopedia of psychology.* John Wiley & Sons. https://doi.org/10.1002/9780470479216.corpsy0491

Oke, T. R. (1981). Canyon geometry and the nocturnal urban heat island: Comparison of scale model and field observations. *Journal of Climatology, 1*(3), 237–254. https://doi.org/10.1002/joc.3370010304

Oke, T. R. (1982). The energetic basis of the urban heat island. *Quarterly Journal of the Royal Meteorological Society, 108*(455), 1–24. https://doi.org/10.1002/qj.49710845502

Peng, S., Piao, S., Ciais, P., Friedlingstein, P., Ottle, C., Bréon, F.-M., Nan, H., Zhou, L., & Myneni, R. B. (2012). Surface urban heat island across 419 global big cities. *Environmental Science & Technology, 46*(2), 696–703. https://doi.org/10.1021/es2030438

Planning Authority Malta. (2020). *State of the environment report 2020.* https://www.pa.org.mt/

Ramamurthy, P., & Sangobanwo, M. (2016). Inter-annual variability in urban heat island intensity over 10 major cities in the United States. *Sustainable Cities and Society, 26*, 65–75. https://doi.org/10.1016/j.scs.2016.05.012

Salmi, T., Määttä, A., Anttila, P., Ruoho-Airola, T., & Amnell, T. (2002). *Detecting trends of annual values of atmospheric pollutants by the Mann-Kendall test and Sen's slope estimates: The Excel template application MAKESENS* (Publications on Air Quality No. 31). Finnish Meteorological Institute.

Santamouris, M. (2013). Using cool pavements as a mitigation strategy to fight urban heat island: A review of the actual developments. *Renewable and Sustainable Energy Reviews, 26*, 224–240. https://doi.org/10.1016/j.rser.2013.05.047

Santamouris, M., Cartalis, C., Synnefa, A., & Kolokotsa, D. (2015). On the impact of urban heat island and global warming on the power demand and electricity consumption of buildings: A review. *Energy and Buildings, 98*, 119–124. https://doi.org/10.1016/j.enbuild.2014.09.052

Sen, P. K. (1968). Estimates of the regression coefficient based on Kendall's tau. *Journal of the American Statistical Association, 63*(324), 1379–1389. https://doi.org/10.1080/01621459.1968.10480934

Seneviratne, S. I., Zhang, X., Adnan, M., Badi, W., Dereczynski, C., Di Luca, A., Ghosh, S., Iskandar, I., Kossin, J., Lewis, S., Otto, F., Pinto, I., Satoh, M., Vicente-Serrano, S. M., Wehner, M., & Zhou, B. (2021). Weather and climate extreme events in a changing climate. In V. Masson-Delmotte, P. Zhai, A. Pirani, S. L. Connors, C. Péan, S. Berger, N. Caud, Y. Chen, L. Goldfarb, M. I. Gomis, M. Huang, K. Leitzell, E. Lonnoy, J. B. R. Matthews, T. K. Maycock, T. Waterfield, O. Yelekçi, R. Yu, & B. Zhou (Eds.), *Climate change 2021: The physical science basis. Contribution of Working Group I to the Sixth Assessment Report of the Intergovernmental Panel on Climate Change* (pp. 1513–1766). Cambridge University Press. https://doi.org/10.1017/9781009157896.013

Shepherd, J. M. (2005). A review of current investigations of urban-induced rainfall and recommendations for the future. *Earth Interactions, 9*(12), 1–27. https://doi.org/10.1175/EI156.1

Sobrino, J. A., Jiménez-Muñoz, J. C., & Paolini, L. (2004). Land surface temperature retrieval from Landsat TM 5. *Remote Sensing of Environment, 90*(4), 434–440. https://doi.org/10.1016/j.rse.2004.02.003

Takane, Y., Kikegawa, Y., Hara, M., & Grimmond, C. S. B. (2019). Urban warming and future air-conditioning use in an Asian megacity: Importance of positive feedback. *npj Climate and Atmospheric Science, 2*, Article 39. https://doi.org/10.1038/s41612-019-0096-2

Tucker, C. J. (1979). Red and photographic infrared linear combinations for monitoring vegetation. *Remote Sensing of Environment, 8*(2), 127–150. https://doi.org/10.1016/0034-4257(79)90013-0

United Nations, Department of Economic and Social Affairs. (2018, May 16). *68% of the world population projected to live in urban areas by 2050, says UN.* https://www.un.org/development/desa/en/news/population/2018-revision-of-world-urbanization-prospects.html

United States Environmental Protection Agency. (2025, September 2). *What are heat islands?* https://www.epa.gov/heatislands/what-are-heat-islands

U.S. Geological Survey. (n.d.). *Landsat Collection 2 Surface Temperature*. Retrieved May 22, 2026, from https://www.usgs.gov/landsat-missions/landsat-collection-2-surface-temperature

Voogt, J. A., & Oke, T. R. (2003). Thermal remote sensing of urban climates. *Remote Sensing of Environment, 86*(3), 370–384. https://doi.org/10.1016/S0034-4257(03)00079-8

Wan, Z., Hook, S., & Hulley, G. (2021). *MODIS/Terra Land Surface Temperature/Emissivity Daily L3 Global 1 km SIN Grid V061* [Data set]. NASA EOSDIS Land Processes DAAC. https://doi.org/10.5067/MODIS/MOD11A1.061

Weng, Q., Lu, D., & Schubring, J. (2004). Estimation of land surface temperature–vegetation abundance relationship for urban heat island studies. *Remote Sensing of Environment, 89*(4), 467–483. https://doi.org/10.1016/j.rse.2003.11.005

Wilks, D. S. (2011). *Statistical methods in the atmospheric sciences* (3rd ed.). Academic Press.

World Meteorological Organization. (2025a, January 10). *WMO confirms 2024 as warmest year on record at about 1.55°C above pre-industrial level.* https://wmo.int/news/media-centre/wmo-confirms-2024-warmest-year-record-about-155degc-above-pre-industrial-level

World Meteorological Organization. (2025b). *WMO global annual to decadal climate update: 2025–2029.* https://wmo.int/resources/publication-series/wmo-global-annual-decadal-climate-update/wmo-global-annual-decadal-climate-update-2025-2029

Xian, G., & Crane, M. (2006). An analysis of urban thermal characteristics and associated land cover in Tampa Bay and Las Vegas using Landsat satellite data. *Remote Sensing of Environment, 104*(2), 147–156. https://doi.org/10.1016/j.rse.2005.09.023

Yang, J., Xin, J., Zhang, Y., Xiao, X., & Xia, J. C. (2022). Contributions of sea–land breeze and local climate zones to daytime and nighttime heat island intensity. *npj Urban Sustainability, 2*, Article 12. https://doi.org/10.1038/s42949-022-00055-z

Yang, Q., Xu, Y., Wen, D., Hu, T., Chakraborty, T., Liu, Y., Yao, R., & others. (2024). Satellite clear-sky observations overestimate surface urban heat islands in humid cities. *Geophysical Research Letters, 51*(2), Article e2023GL106995. https://doi.org/10.1029/2023GL106995

Yavuzturk, C., Ksaibati, K., & Chiasson, A. D. (2005). Assessment of temperature fluctuations in asphalt pavements due to thermal environmental conditions using a two-dimensional transient finite-difference approach. *Journal of Materials in Civil Engineering, 17*(4), 465–475. https://doi.org/10.1061/(ASCE)0899-1561(2005)17:4(465)

Yuan, F., & Bauer, M. E. (2007). Comparison of impervious surface area and normalized difference vegetation index as indicators of surface urban heat island effects in Landsat imagery. *Remote Sensing of Environment, 106*(3), 375–386. https://doi.org/10.1016/j.rse.2006.09.003

Yue, S., Pilon, P., & Cavadias, G. (2002). Power of the Mann–Kendall and Spearman's rho tests for detecting monotonic trends in hydrological series. *Journal of Hydrology, 259*(1–4), 254–271. https://doi.org/10.1016/S0022-1694(01)00594-7

Zhao, L., Lee, X., Smith, R. B., & Oleson, K. (2014). Strong contributions of local background climate to urban heat islands. *Nature, 511*(7508), 216–219. https://doi.org/10.1038/nature13462

Zheng, Z., Ren, C., Shi, Y., Lau, K. K.-L., & Ng, E. (2024). Effects of urbanization and topography on thermal comfort during a heat wave event: A case study of Fuzhou, China. *Sustainable Cities and Society, 101*, Article 105154. https://doi.org/10.1016/j.scs.2024.105154

Zhou, Y., Guan, H., Huang, C., Fan, L., Gharib, S., Batelaan, O., & Simmons, C. (2019). Sea breeze cooling capacity and its influencing factors in a coastal city. *Building and Environment, 166*, Article 106408. https://doi.org/10.1016/j.buildenv.2019.106408

8. Appendix

8.1 Extra figures and tables

Table A1. Annual ISA-based rural and urban mean LST values for Malta and Zaragoza, 2013–2025.

Site	Year	Rural mean LST (°C)	Urban mean LST (°C)	Urban - rural LST difference (°C)
Malta	2013	47.1	45.2	-1.9
Malta	2014	44.55	43.05	-1.49
Malta	2015	46.21	45.55	-0.65
Malta	2016	42.99	40.98	-2.01
Malta	2017	44.46	42.89	-1.58
Malta	2018	47.57	46.37	-1.2
Malta	2019	44.22	43.18	-1.04
Malta	2020	43.51	43.22	-0.29
Malta	2021	47.07	45	-2.07
Malta	2022	47.86	46.08	-1.78
Malta	2023	45.18	44.9	-0.27
Malta	2024	46.99	45.1	-1.9
Malta	2025	43.43	42.37	-1.06
Zaragoza	2013	36.11	37.87	1.77
Zaragoza	2014	36.97	38.73	1.76
Zaragoza	2015	40.02	41.26	1.24
Zaragoza	2016	38.81	40.54	1.74
Zaragoza	2017	42.59	45.42	2.83
Zaragoza	2018	43.97	46.15	2.18
Zaragoza	2019	43.79	45.89	2.1
Zaragoza	2020	34.54	38.57	4.02
Zaragoza	2021	38.81	41.74	2.93
Zaragoza	2022	43.66	45.78	2.12

Zaragoza	2023	48.37	49.73	1.35
Zaragoza	2024	46.81	48.98	2.17
Zaragoza	2025	39.29	40.54	1.25

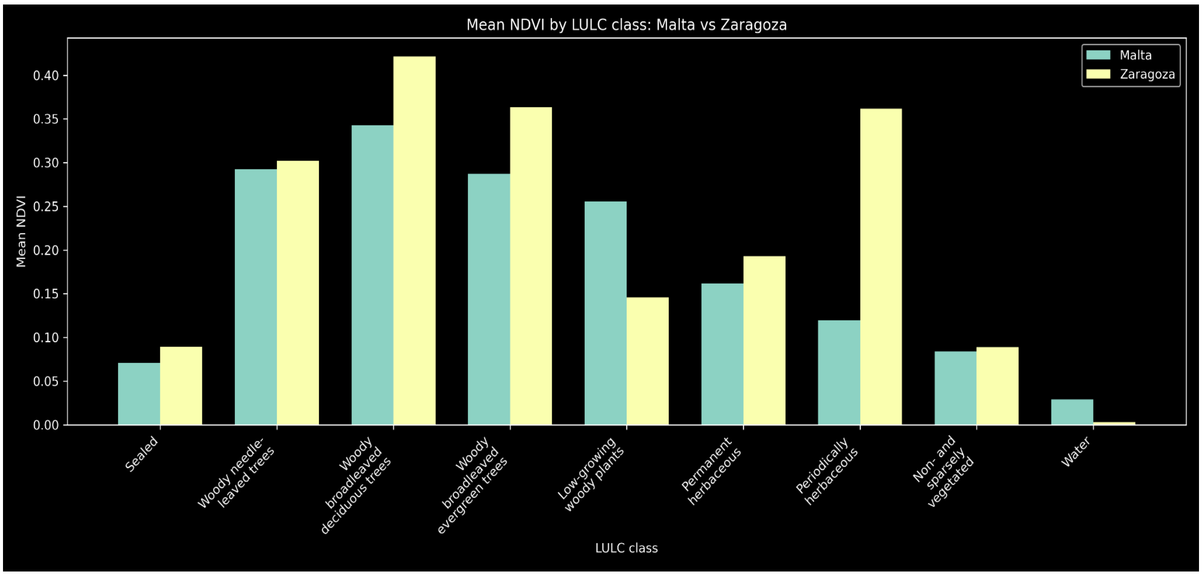

Figure 1a. Mean NDVI by stable LULC class in Malta and Zaragoza, 2015–2025. The Mean NDVI values were extracted from the average NDVI raster for each stable LULC class. Higher NDVI values indicate stronger vegetation presence, while lower values indicate sealed, sparsely vegetated, water, or non-vegetated surfaces. The comparison shows how vegetation density differs between land-cover classes and between the maritime study area of Malta and the inland study area of Zaragoza. For every single class except “Low-growing woody plants” & “Water”, the mean NDVI is higher in Zaragoza than in Malta, and the highest NDVI values are displayed in “Woody broadleaved deciduous trees”.

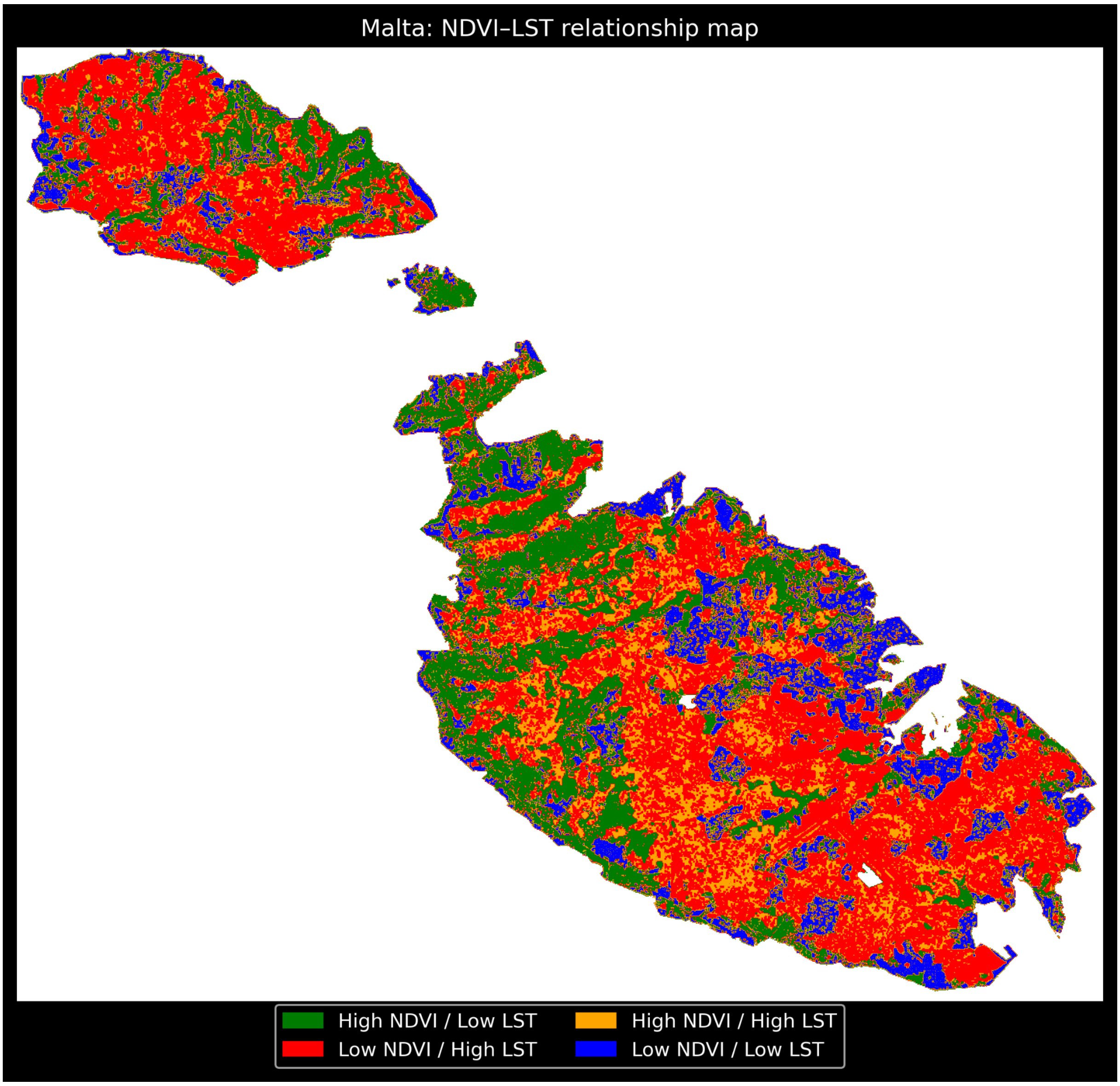

Figure 2a. Raster of the NDVI-LST relationship on Malta. All valid pixels were divided according to whether their NDVI and LST values were above or below the median. This has led to 4 classes: high NDVI/low LST, low NDVI/high LST, high NDVI/high LST, and low NDVI/low LST. It is important to note that this map represents relative internal patterns, as the median thresholds are calculated separately for Figures 17 and 18. So spatial logic can be drawn out from looking at these figures, but they are not directly comparable classes.

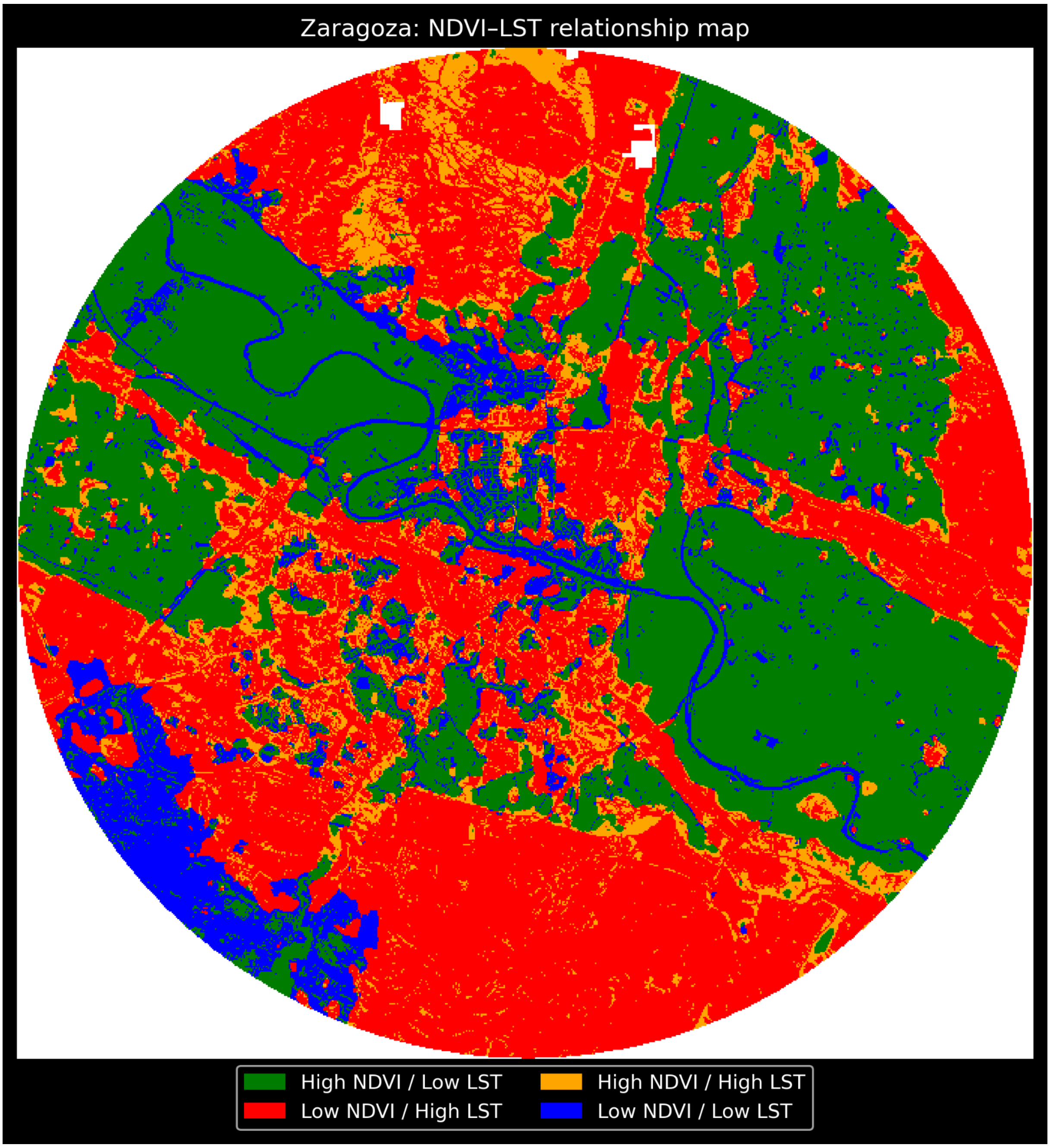

Figure 2b. Raster of the NDVI-LST relationship in Zaragoza. All valid pixels were divided according to whether their NDVI and LST values were above or below the median. This has led to 4 classes: high NDVI/low LST, low NDVI/high LST, high NDVI/high LST, and low NDVI/low LST. It is important to note that this map represents relative internal patterns, as the median thresholds are calculated separately for Figures 17 and 18. So spatial logic can be drawn out from looking at these figures, but they are not directly comparable classes.

8.2 Code

The AI-generated Google Earth Engine script used to calculate daytime and nighttime SUHI intensity from MODIS MOD11A1 data is provided below. The script filters daily MODIS LST images for the summer months, applies quality-control filtering, converts MODIS scaled digital numbers to degrees Celsius, extracts mean LST values for ISA-based urban and rural masks, and exports daily and annual SUHI tables. For personal privacy, the exact file paths and layer names are replaced with placeholders.

Input	Description	Example placeholder
Study area boundary	Malta national boundary or Zaragoza 10 km ISA raster extent	YOUR_STUDY_AREA_BOUNDARY_ASSET
ISA class raster	Raster where rural = 1 and urban = 2	YOUR_ISA_CLASS_RASTER_ASSET
MODIS product	MOD11A1 Collection 6.1	MODIS/061/MOD11A1
Study period	Years analysed	2003–2025
Season	Summer months	June, July, August

```
// =============================================================
// MODIS SUHI ANALYSIS — ANONYMISED GOOGLE EARTH ENGINE SCRIPT
// =============================================================
// Purpose:
// Calculates daytime and nighttime SUHI from MODIS MOD11A1 LST
// using an uploaded study-area boundary and an uploaded ISA-based
// urban/rural classification raster.
// =============================================================


// =============================================================
// 1. USER PARAMETERS
// =============================================================

// Use a generic label when exporting outputs.
// Replace only inside GEE with your own preferred label.
var SITE_LABEL = 'STUDY_AREA';

// Study period
var START_YEAR = 2003;
var END_YEAR = 2025;

// Summer months: June, July, August
var SUMMER_MONTHS = [6, 7, 8];

// MODIS scale
var MODIS_SCALE = 1000;

// Export CRS can be left blank unless you need a specific projection.
// var EXPORT_CRS = 'EPSG:3035';


// =============================================================
// 2. LOAD STUDY AREA AND URBAN/RURAL MASK
// =============================================================

// Replace this placeholder with your uploaded study-area boundary asset.
var studyArea = ee.FeatureCollection('YOUR_STUDY_AREA_BOUNDARY_ASSET');

// Replace this placeholder with your uploaded ISA class raster asset.
```

```
// The raster should contain:
// class 1 = rural
// class 2 = urban
var isaClass = ee.Image('YOUR_ISA_CLASS_RASTER_ASSET');

// Geometry used for reductions and exports
var geometry = studyArea.geometry();

// Urban/rural masks from ISA classification
var ruralMask = isaClass.eq(1);
var urbanMask = isaClass.eq(2);

// Visual check
Map.centerObject(studyArea, 9);
Map.addLayer(studyArea, {color: 'cyan'}, 'Study area boundary');
Map.addLayer(ruralMask.selfMask().clip(geometry), {palette: ['green']}, 'Rural mask');
Map.addLayer(urbanMask.selfMask().clip(geometry), {palette: ['red']}, 'Urban mask');


// ============================================================
// 3. LOAD MODIS MOD11A1 AND APPLY QUALITY CONTROL
// ============================================================

// MODIS MOD11A1 contains:
// LST_Day_1km
// LST_Night_1km
// QC_Day
// QC_Night
//
// QC bits 0–1 equal to 00 indicate good-quality LST retrievals.

function prepareMODIS(img) {
  var date = ee.Date(img.get('system:time_start'));

  // Daytime quality mask
  var qcDay = img.select('QC_Day');
  var goodDay = qcDay.bitwiseAnd(3).eq(1);

  // Nighttime quality mask
  var qcNight = img.select('QC_Night');
  var goodNight = qcNight.bitwiseAnd(3).eq(1);

  // Convert daytime LST from scaled DN to Celsius
  var day = img.select('LST_Day_1km')
    .updateMask(goodDay)
    .multiply(0.02)
    .subtract(273.15)
    .rename('LST_day');

  // Convert nighttime LST from scaled DN to Celsius
  var night = img.select('LST_Night_1km')
    .updateMask(goodNight)
    .multiply(0.02)
    .subtract(273.15)
    .rename('LST_night');

  return ee.Image.cat(day, night)
    .copyProperties(img, ['system:time_start'])
    .set('date', date.format('YYYY-MM-dd'))
    .set('year', date.get('year'))
    .set('month', date.get('month'));
}
```

```
var modis = ee.ImageCollection('MODIS/061/MOD11A1')
  .filterDate(START_YEAR + '-01-01', END_YEAR + '-12-31')
  .filterBounds(geometry)
  .map(prepareMODIS);


// ============================================================
// 4. FILTER TO SUMMER MONTHS
// ============================================================

var lstSummer = modis.filter(
  ee.Filter.inList('month', SUMMER_MONTHS)
);

print('Summer MODIS image count:', lstSummer.size());


// ============================================================
// 5. FUNCTION TO EXTRACT MEAN LST
// ============================================================

function reduceMean(image, bandName) {
  return image.reduceRegion({
    reducer: ee.Reducer.mean(),
    geometry: geometry,
    scale: MODIS_SCALE,
    maxPixels: 1e13,
    bestEffort: true
  }).get(bandName);
}

function safeSubtract(a, b) {
  return ee.Algorithms.If(
    ee.Algorithms.IsEqual(a, null),
    null,
    ee.Algorithms.If(
      ee.Algorithms.IsEqual(b, null),
      null,
      ee.Number(a).subtract(ee.Number(b))
    )
  );
}


// ============================================================
// 6. CALCULATE DAILY URBAN, RURAL, AND SUHI VALUES
// ============================================================

var dailyResults = lstSummer.map(function(img) {

  var day = img.select('LST_day');
  var night = img.select('LST_night');

  // Apply masks
  var urbanDay = day.updateMask(urbanMask);
  var ruralDay = day.updateMask(ruralMask);

  var urbanNight = night.updateMask(urbanMask);
  var ruralNight = night.updateMask(ruralMask);

  // Extract means
```

```
  var urbanDayMean = reduceMean(urbanDay, 'LST_day');
  var ruralDayMean = reduceMean(ruralDay, 'LST_day');

  var urbanNightMean = reduceMean(urbanNight, 'LST_night');
  var ruralNightMean = reduceMean(ruralNight, 'LST_night');

  // SUHI = urban LST - rural LST
  var suhiDay = safeSubtract(urbanDayMean, ruralDayMean);
  var suhiNight = safeSubtract(urbanNightMean, ruralNightMean);

  return ee.Feature(null, {
    site: SITE_LABEL,
    date: img.get('date'),
    year: img.get('year'),
    month: img.get('month'),

    urban_day_LST_C: urbanDayMean,
    rural_day_LST_C: ruralDayMean,
    SUHI_day_C: suhiDay,

    urban_night_LST_C: urbanNightMean,
    rural_night_LST_C: ruralNightMean,
    SUHI_night_C: suhiNight
  });
});

print('Daily SUHI results:', dailyResults.limit(10));


// ============================================================
// 7. CREATE ANNUAL SUMMER MEAN SUHI TABLE
// ============================================================

var years = ee.List.sequence(START_YEAR, END_YEAR);

var annualResults = ee.FeatureCollection(
  years.map(function(year) {
    year = ee.Number(year);

    var subset = dailyResults.filter(
      ee.Filter.eq('year', year)
    );

    return ee.Feature(null, {
      site: SITE_LABEL,
      year: year,

      urban_day_LST_C: subset.aggregate_mean('urban_day_LST_C'),
      rural_day_LST_C: subset.aggregate_mean('rural_day_LST_C'),
      SUHI_day_C: subset.aggregate_mean('SUHI_day_C'),

      urban_night_LST_C: subset.aggregate_mean('urban_night_LST_C'),
      rural_night_LST_C: subset.aggregate_mean('rural_night_LST_C'),
      SUHI_night_C: subset.aggregate_mean('SUHI_night_C'),

      valid_observations: subset.size()
    });
  })
);

print('Annual SUHI results:', annualResults);
```

```
// ============================================================
// 8. CREATE ANNUAL MEAN LST MAPS
// ============================================================

function annualMeanImage(year) {
  year = ee.Number(year);

  var annualCollection = lstSummer.filter(
    ee.Filter.eq('year', year)
  );

  var meanDay = annualCollection
    .select('LST_day')
    .mean()
    .clip(geometry)
    .rename('LST_day_mean_C');

  var meanNight = annualCollection
    .select('LST_night')
    .mean()
    .clip(geometry)
    .rename('LST_night_mean_C');

  return meanDay
    .addBands(meanNight)
    .set('year', year)
    .set('site', SITE_LABEL);
}

var annualMeanImages = ee.ImageCollection(
  years.map(function(year) {
    return annualMeanImage(year);
  })
);

print('Annual mean LST images:', annualMeanImages);


// ============================================================
// 9. VISUALISE ONE EXAMPLE YEAR
// ============================================================

var exampleYear = 2023;

var exampleDay = annualMeanImages
  .filter(ee.Filter.eq('year', exampleYear))
  .first()
  .select('LST_day_mean_C');

var visParams = {
  min: 20,
  max: 50,
  palette: ['blue', 'cyan', 'green', 'yellow', 'orange', 'red']
};

Map.addLayer(
  exampleDay,
  visParams,
  'Example annual mean daytime LST'
);
```

```
// ================================================================
// 10. EXPORT DAILY SUHI TABLE
// ================================================================

Export.table.toDrive({
  collection: dailyResults,
  description: SITE_LABEL + '_MODIS_SUHI_Daily_Table',
  fileFormat: 'CSV',
  selectors: [
    'site',
    'date',
    'year',
    'month',
    'urban_day_LST_C',
    'rural_day_LST_C',
    'SUHI_day_C',
    'urban_night_LST_C',
    'rural_night_LST_C',
    'SUHI_night_C'
  ]
});


// ================================================================
// 11. EXPORT ANNUAL SUHI TABLE
// ================================================================

Export.table.toDrive({
  collection: annualResults,
  description: SITE_LABEL + '_MODIS_SUHI_Annual_Table',
  fileFormat: 'CSV',
  selectors: [
    'site',
    'year',
    'urban_day_LST_C',
    'rural_day_LST_C',
    'SUHI_day_C',
    'urban_night_LST_C',
    'rural_night_LST_C',
    'SUHI_night_C',
    'valid_observations'
  ]
});


// ================================================================
// 12. OPTIONAL: EXPORT ANNUAL MEAN DAYTIME AND NIGHTTIME LST RASTERS
// ================================================================
// This exports one GeoTIFF per year with two bands:
// band 1 = annual summer mean daytime LST
// band 2 = annual summer mean nighttime LST

/*
years.getInfo().forEach(function(year) {

  var image = annualMeanImage(year);

  Export.image.toDrive({
    image: image,
    description: SITE_LABEL + '_MODIS_Annual_Mean_LST_' + year,
    region: geometry,
```

```
    scale: MODIS_SCALE,
    maxPixels: 1e13,
    fileFormat: 'GeoTIFF'
  });

});
*/
```

```
// ============================================================
// 13. OPTIONAL: EXPORT ONE SPECIFIC EXAMPLE YEAR RASTER
// ============================================================

/*
Export.image.toDrive({
  image: annualMeanImage(exampleYear),
  description: SITE_LABEL + '_MODIS_Annual_Mean_LST_Example_Year',
  region: geometry,
  scale: MODIS_SCALE,
  maxPixels: 1e13,
  fileFormat: 'GeoTIFF'
});
*/
```

Code used to generate the MODIS UHI trendline graphs in Arc GIS Pro

This ArcGIS Pro Python script was used to create the MODIS summer UHI trendline figures for Malta and Zaragoza. It reads the annual UHI CSV files exported from Google Earth Engine, separates daytime and nighttime UHI values, calculates linear regression trends, and plots the annual UHI time series with trendlines. The figure legend reports the slope and p-value for each trend, and a separate CSV file is exported containing the full regression statistics. Personal file paths have been replaced with placeholders for reproducibility.

```
import pandas as pd
import matplotlib.pyplot as plt
from scipy.stats import linregress
import os

# ============================================================
# INPUTS — REPLACE THESE PLACEHOLDERS
# ============================================================

malta_csv = r"PATH_TO_MALTA_MODIS_SUHI_ANNUAL_CSV.csv"
zaragoza_csv = r"PATH_TO_ZARAGOZA_MODIS_SUHI_ANNUAL_CSV.csv"

output_folder = r"PATH_TO_OUTPUT_FIGURE_FOLDER"
os.makedirs(output_folder, exist_ok=True)

# Expected CSV columns:
# site
# year
# urban_day_LST_C
# rural_day_LST_C
# SUHI_day_C
# urban_night_LST_C
```

```
# rural_night_LST_C
# SUHI_night_C


# ==============================================================
# FUNCTION TO CREATE TRENDLINE FIGURE
# ==============================================================

def create_uhi_trend_figure(csv_path, site_name, output_folder):
    """
    Creates a MODIS summer daytime and nighttime UHI trendline graph
    for one study area.

    The graph includes:
    - annual daytime UHI values
    - annual nighttime UHI values
    - linear trendlines
    - slope and p-value in the legend
    - saved high-resolution PNG
    - saved statistics CSV
    """

    # ------------------------------------------------------------
    # Load data
    # ------------------------------------------------------------

    df = pd.read_csv(csv_path)

    print("\n" + "=" * 70)
    print(f"Processing {site_name}")
    print("=" * 70)

    print("Columns in CSV:")
    print(df.columns.tolist())

    # Keep only selected site if site column exists
    if "site" in df.columns:
        df = df[df["site"].astype(str).str.lower() == site_name.lower()].copy()

    # Convert relevant columns to numeric
    df["year"] = pd.to_numeric(df["year"], errors="coerce")
    df["SUHI_day_C"] = pd.to_numeric(df["SUHI_day_C"], errors="coerce")
    df["SUHI_night_C"] = pd.to_numeric(df["SUHI_night_C"], errors="coerce")

    # Sort by year
    df = df.dropna(subset=["year"]).copy()
    df = df.sort_values("year")

    # Separate valid day and night records
    day_df = df.dropna(subset=["SUHI_day_C"]).copy()
    night_df = df.dropna(subset=["SUHI_night_C"]).copy()

    print("Valid daytime rows:", len(day_df))
    print("Valid nighttime rows:", len(night_df))

    if len(day_df) < 2:
        raise RuntimeError(f"Not enough valid daytime UHI values for {site_name}.")

    if len(night_df) < 2:
        raise RuntimeError(f"Not enough valid nighttime UHI values for {site_name}.")

    # ------------------------------------------------------------
```

```
# Linear trend calculations
# ------------------------------------------------------------

day_lr = linregress(day_df["year"], day_df["SUHI_day_C"])
night_lr = linregress(night_df["year"], night_df["SUHI_night_C"])

day_trend = day_lr.intercept + day_lr.slope * day_df["year"]
night_trend = night_lr.intercept + night_lr.slope * night_df["year"]

# ------------------------------------------------------------
# Save trend statistics
# ------------------------------------------------------------

stats = pd.DataFrame([
    {
        "Study area": site_name,
        "UHI period": "Daytime UHI",
        "Linear slope (°C/year)": round(day_lr.slope, 4),
        "Intercept": round(day_lr.intercept, 4),
        "Pearson r": round(day_lr.rvalue, 4),
        "Linear R²": round(day_lr.rvalue ** 2, 4),
        "Linear p-value": round(day_lr.pvalue, 4),
        "Standard error": round(day_lr.stderr, 4)
    },
    {
        "Study area": site_name,
        "UHI period": "Nighttime UHI",
        "Linear slope (°C/year)": round(night_lr.slope, 4),
        "Intercept": round(night_lr.intercept, 4),
        "Pearson r": round(night_lr.rvalue, 4),
        "Linear R²": round(night_lr.rvalue ** 2, 4),
        "Linear p-value": round(night_lr.pvalue, 4),
        "Standard error": round(night_lr.stderr, 4)
    }
])

stats_csv = os.path.join(
    output_folder,
    f"{site_name}_MODIS_Summer_UHI_Trend_Statistics.csv"
)

stats.to_csv(stats_csv, index=False)

print("\nTrend statistics:")
print(stats)

# ------------------------------------------------------------
# Create figure
# ------------------------------------------------------------

plt.figure(figsize=(13, 7))

# Daytime UHI line
plt.plot(
    day_df["year"],
    day_df["SUHI_day_C"],
    marker="o",
    linewidth=2.2,
    label="Daytime UHI"
)

# Daytime trendline
```

```
plt.plot(
    day_df["year"],
    day_trend,
    linestyle="--",
    linewidth=2,
    label=f"Daytime trend: {day_lr.slope:.3f} °C/year, p = {day_lr.pvalue:.3f}"
)

# Nighttime UHI line
plt.plot(
    night_df["year"],
    night_df["SUHI_night_C"],
    marker="s",
    linewidth=2.2,
    label="Nighttime UHI"
)

# Nighttime trendline
plt.plot(
    night_df["year"],
    night_trend,
    linestyle="--",
    linewidth=2,
    label=f"Nighttime trend: {night_lr.slope:.3f} °C/year, p = {night_lr.pvalue:.3f}"
)

# Zero reference line
plt.axhline(
    y=0,
    linewidth=1,
    alpha=0.7
)

# Labels and title
plt.title(
    f"{site_name} MODIS Summer UHI Trends, 2003–2025",
    fontsize=16,
    fontweight="bold"
)

plt.xlabel("Year", fontsize=13)
plt.ylabel("UHI intensity (°C)", fontsize=13)

plt.xticks(
    df["year"].astype(int).unique(),
    rotation=45
)

plt.grid(True, alpha=0.3)
plt.legend(fontsize=10)

plt.tight_layout()

# ------------------------------------------------------------
# Save figure
# ------------------------------------------------------------

output_png = os.path.join(
    output_folder,
    f"{site_name}_MODIS_Summer_UHI_Trends_Day_Night.png"
)
```

```
    plt.savefig(output_png, dpi=300, bbox_inches="tight")
    plt.show()

    print("\nFigure saved here:")
    print(output_png)

    print("\nStatistics CSV saved here:")
    print(stats_csv)


# ============================================================
# RUN FOR MALTA AND ZARAGOZA
# ============================================================

create_uhi_trend_figure(
    csv_path=malta_csv,
    site_name="Malta",
    output_folder=output_folder
)

create_uhi_trend_figure(
    csv_path=zaragoza_csv,
    site_name="Zaragoza",
    output_folder=output_folder
)

print("\nFinished creating MODIS UHI trendline figures.")
```

Code used to generate the mean NDVI by stable LULC class in Malta and Zaragoza graph in Arc GIS Pro

```
import arcpy
import os
import pandas as pd
import matplotlib.pyplot as plt

# ============================================================
# SETTINGS — REPLACE PLACEHOLDERS
# ============================================================

arcpy.env.overwriteOutput = True
arcpy.CheckOutExtension("Spatial")

# Optional: set your project geodatabase if your rasters are stored there
project_gdb = r"PATH_TO_YOUR_PROJECT_GEODATABASE.gdb"
arcpy.env.workspace = project_gdb

# Output folder
output_folder = r"PATH_TO_OUTPUT_FOLDER"
os.makedirs(output_folder, exist_ok=True)

output_csv = os.path.join(output_folder, "Mean_NDVI_by_Stable_LULC_Class.csv")
output_png = os.path.join(output_folder, "Mean_NDVI_by_Stable_LULC_Class_Malta_Zaragoza.png")

# ============================================================
# INPUT RASTERS — REPLACE WITH YOUR OWN RASTER NAMES OR PATHS
# ============================================================

inputs = {
```

```
    "Malta": {
        "ndvi": r"PATH_OR_RASTER_NAME_TO_MALTA_AVERAGE_NDVI",
        "lulc": r"PATH_OR_RASTER_NAME_TO_MALTA_STABLE_LULC"
    },
    "Zaragoza": {
        "ndvi": r"PATH_OR_RASTER_NAME_TO_ZARAGOZA_AVERAGE_NDVI",
        "lulc": r"PATH_OR_RASTER_NAME_TO_ZARAGOZA_STABLE_LULC"
    }
}

# ============================================================
# CLC+ BACKBONE CLASS NAMES
# Adjust if your raster uses different class codes
# ============================================================

class_names = {
    1: "Sealed",
    2: "Needleleaf trees",
    3: "Broadleaf deciduous trees",
    4: "Broadleaf evergreen trees",
    5: "Low-growing woody plants",
    6: "Permanent herbaceous",
    7: "Periodically herbaceous",
    9: "Non/sparsely vegetated",
    10: "Water"
}

# ============================================================
# HELPER FUNCTIONS
# ============================================================

def find_dataset(name_or_path):
    """
    Finds a raster either by full path, geodatabase name, or active map layer name.
    """

    if arcpy.Exists(name_or_path):
        return name_or_path

    gdb_path = os.path.join(project_gdb, name_or_path)
    if arcpy.Exists(gdb_path):
        return gdb_path

    # Search active map layers
    aprx = arcpy.mp.ArcGISProject("CURRENT")
    active_map = aprx.activeMap

    if active_map:
        for lyr in active_map.listLayers():
            if lyr.name.lower() == str(name_or_path).lower():
                try:
                    return arcpy.Describe(lyr).catalogPath
                except:
                    try:
                        return lyr.dataSource
                    except:
                        return lyr.name

    raise RuntimeError(f"Could not find dataset: {name_or_path}")


def get_zone_field(zone_raster):
```

```
    """
    Finds the correct raster value field for the LULC raster.
    """

    fields = [f.name for f in arcpy.ListFields(zone_raster)]

    if "VALUE" in fields:
        return "VALUE"
    elif "Value" in fields:
        return "Value"
    elif "value" in fields:
        return "value"
    else:
        return "VALUE"


def zonal_mean_ndvi(site_name, ndvi_raster, lulc_raster):
    """
    Calculates mean NDVI for each stable LULC class.
    """

    print("\n" + "=" * 70)
    print(f"Processing {site_name}")
    print("=" * 70)

    ndvi_raster = find_dataset(ndvi_raster)
    lulc_raster = find_dataset(lulc_raster)

    print(f"NDVI raster: {ndvi_raster}")
    print(f"LULC raster: {lulc_raster}")

    # Match environment to NDVI raster
    arcpy.env.snapRaster = ndvi_raster
    arcpy.env.cellSize = ndvi_raster
    arcpy.env.extent = ndvi_raster

    zone_field = get_zone_field(lulc_raster)

    temp_table = os.path.join(
        arcpy.env.scratchGDB,
        f"zonal_ndvi_{site_name}"
    )

    if arcpy.Exists(temp_table):
        arcpy.management.Delete(temp_table)

    # Zonal statistics: stable LULC classes as zones, NDVI as value raster
    arcpy.sa.ZonalStatisticsAsTable(
        in_zone_data=lulc_raster,
        zone_field=zone_field,
        in_value_raster=ndvi_raster,
        out_table=temp_table,
        ignore_nodata="DATA",
        statistics_type="MEAN"
    )

    fields = [f.name for f in arcpy.ListFields(temp_table)]

    value_field = "VALUE" if "VALUE" in fields else "Value"
    mean_field = "MEAN"
    count_field = "COUNT" if "COUNT" in fields else None
```

```
    cursor_fields = [value_field, mean_field]
    if count_field:
        cursor_fields.append(count_field)

    rows = []

    with arcpy.da.SearchCursor(temp_table, cursor_fields) as cursor:
        for row in cursor:
            class_value = int(row[0])
            mean_ndvi = row[1]
            pixel_count = row[2] if count_field else None

            if class_value in class_names:
                rows.append({
                    "Site": site_name,
                    "LULC class value": class_value,
                    "LULC class": class_names[class_value],
                    "Mean NDVI": mean_ndvi,
                    "Pixel count": pixel_count
                })

    return rows


# ==============================================================
# RUN ZONAL STATISTICS
# ==============================================================

all_rows = []

for site, paths in inputs.items():
    site_rows = zonal_mean_ndvi(
        site_name=site,
        ndvi_raster=paths["ndvi"],
        lulc_raster=paths["lulc"]
    )
    all_rows.extend(site_rows)

df = pd.DataFrame(all_rows)

# Sort by class value
df = df.sort_values(["LULC class value", "Site"])

# Save CSV
df.to_csv(output_csv, index=False)

print("\nMean NDVI table:")
print(df)

print("\nCSV saved here:")
print(output_csv)

# ==============================================================
# PREPARE DATA FOR GRAPH
# ==============================================================

plot_df = df.pivot(
    index="LULC class",
    columns="Site",
    values="Mean NDVI"
)
```

```
# Preserve CLC+ order
ordered_classes = [
    class_names[c] for c in class_names.keys()
    if class_names[c] in plot_df.index
]

plot_df = plot_df.loc[ordered_classes]

# ============================================================
# CREATE GROUPED BAR CHART
# ============================================================

ax = plot_df.plot(
    kind="bar",
    figsize=(14, 7),
    width=0.8
)

plt.title(
    "Mean NDVI by Stable LULC Class in Malta and Zaragoza, 2015–2025",
    fontsize=15,
    fontweight="bold"
)

plt.xlabel("Stable LULC class", fontsize=12)
plt.ylabel("Mean NDVI", fontsize=12)

plt.xticks(rotation=45, ha="right")
plt.ylim(-0.1, 1.0)

plt.grid(axis="y", alpha=0.3)
plt.legend(title="Study area")

plt.tight_layout()

plt.savefig(output_png, dpi=300, bbox_inches="tight")
plt.show()

print("\nFigure saved here:")
print(output_png)

print("\nFinished.")
```